Efficient Electrocatalytic Reduction of CO_2

2018/1/27 Literature Seminar
M1 Takehiro Kato

Use of One-Carbon Molecules

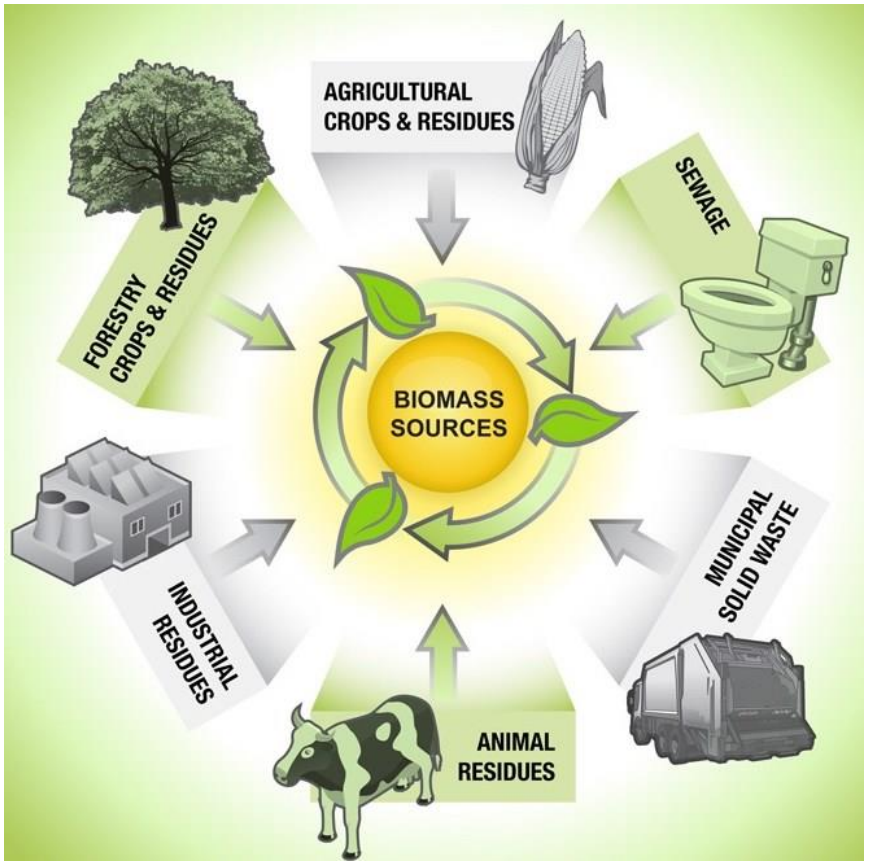

EtOH, MeOH, CH_4, …

Reduction of CO_2 to One-Carbon Molecules

$CO_2 + 2H^+ + 2e^-$ → $CO + H_2O$

$E^0 = -0.53$ V

$\Delta G^0 = 24.5$ kcal/mol

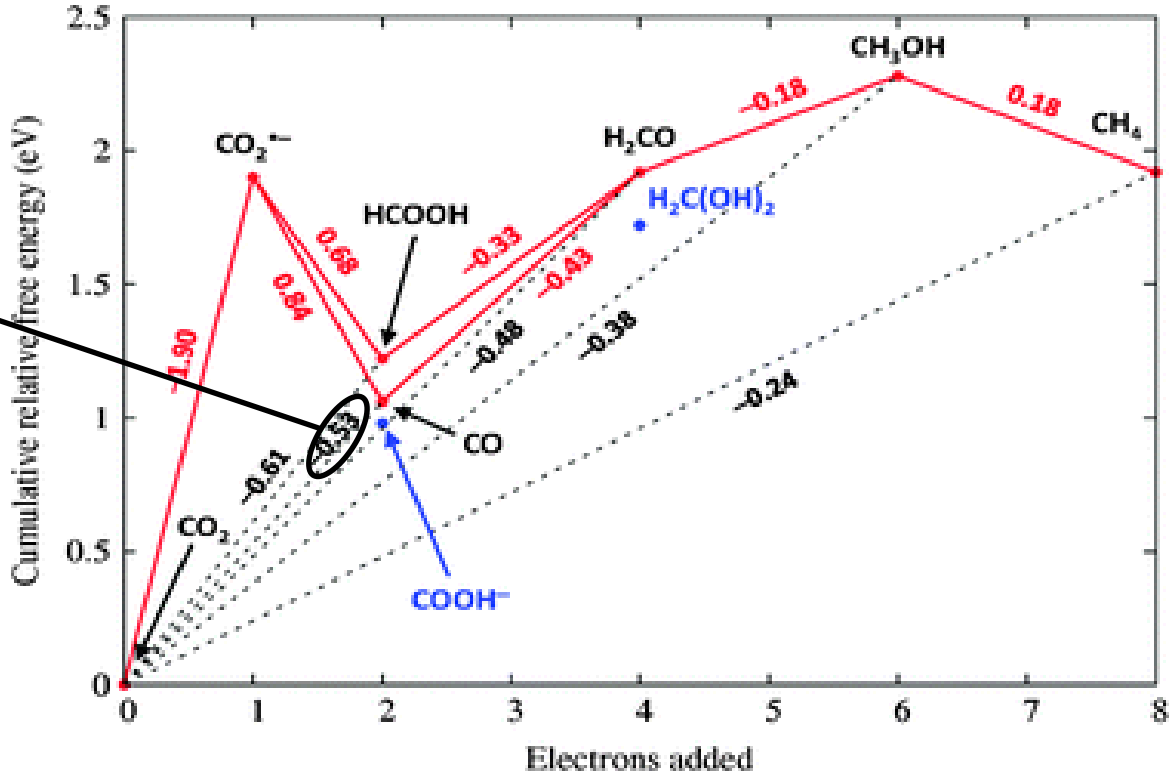

Frost diagram for multi-electron and multi-proton reduction of CO_2 at pH 7.

→ **Reduction of CO_2 is very uphill reaction.**
Electronic or/and catalytic approach is needed.

Schneider, J.; Jia, H.; Muckerman, J. T.; Fujita, E. *Chem. Soc. Rev.* **2012**, *41*, 2036.

Drawbacks to Electronic Reduction of CO_2

CO_2 —(conditions)→ CO, HCOOH, ...

conditions	product	current efficiency
Hg pool electrode $LiHCO_3$ aq. pH 6.7, 25 °C	$HCOO^-$	98%[1)]
Hg pool electrode $Fe^{III}(TPP)Cl$, CF_3CH_2OH DMF, Et_4NClO_4 -1.5 V*, 20 °C	CO (TOF: 350 h^{-1})	96%[2)]
carbon cloth electrode $[Rh^{III}(bpy)_2Cl_2]^+(ClO_4^-$ salt?) *n*-Bu_4NPF_6, MeCN -1.31 V*, 1 h	$HCOO^-$ H_2 (TON: 8.0)	$HCOO^-$: 64%[3)] H_2: 12%

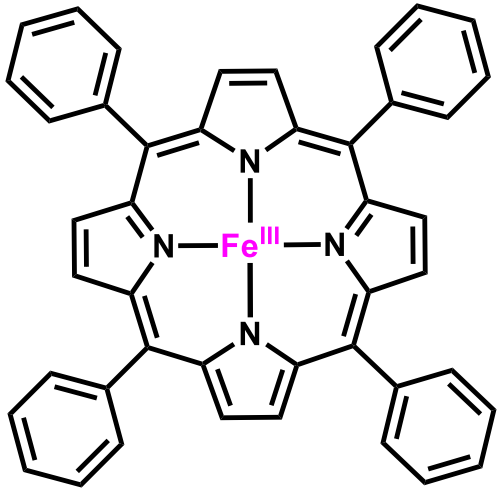

$Fe^{III}(TPP)^+$

*Potentials are vs. SHE.

Problems to be concerned:
current efficiency
voltage to be applied
selectivity over reduction of water

use of heavy metals (Hg, ...)
stability against air and water
stability through long-term and repetitive use

1) Paik, W.; Andersen, T. N.; Eyring, H. *Electrochim. Acta.* **1969**, *14*, 1217. 2) Bhugun, I.; Lexa, D.; Savéant, J. M. *J. Am. Chem. Soc.* **1996**, *118*, 1769. 3) Bolinger, C. M.; Story, N.; Sullivan, B. P.; Meyer, T. J. *Inorg. Chem.* **1988**, *27*, 4582.

Contents

1. Electrocatalytic reduction of CO_2 using nickel complexes in organic media (Chang, 2011)
   Chem. Commun. **2011**, *47*, 6578.

2. Electrocatalytic reduction of CO_2 on covalent organic frameworks (COFs) in water
   (Yaghi and Chang, 2015 and 2017)
   Science **2015**, *349*, 1208.
   J. Am. Chem. Soc. **2018**, *140*, 1116.

Christopher J. Chang

1997 B.S./M.S. Caltech (Prof. H. B. Gray, inorganic catalysis)
2002 Ph.D. MIT (Prof. D. G. Nocera, porphyrins)
2002-2004 Postdoc. MIT (Advisor: S. J. Lippard, fluorescent imaging)
2004-2009 Assistant Prof., UC Berkeley
2009-2012 Associate Prof. , UC Berkeley
2012-present Prof., UC Berkeley

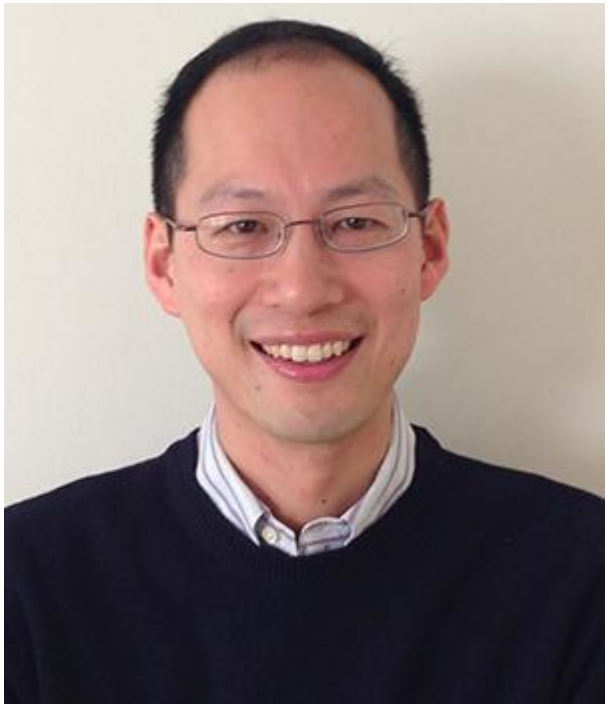

Research topics:
Transition metal signaling
Activity-based sensing
Metals in neurobiology
Artificial photosynthesis

Previous Work with $[Ni^{II}(cyclam)]^{2+}$

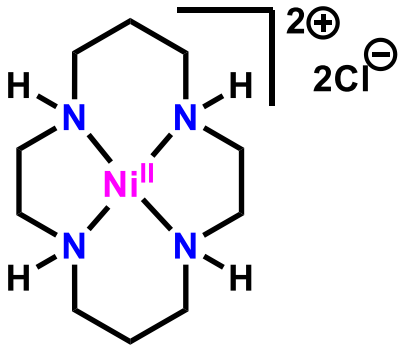

CO_2 → CO (H_2: trace)

0.1 M $KClO_4$ aq., pH = 4.1

-1.00 V (vs. SHE)

Hg cathode

(cyclam = 1,4,8,11-tetraazacyclotetradecane)

TOF: 10^3 h^{-1}

Current Efficiency: up to 99%

↓

Planar, electron-rich ligand could be a good ligand.

Beley, M.; Collin, J. P.; Ruppert, R.; Sauvage, J. P. *J. Am. Chem. Soc.* **1986**, *108*, 7461.

Synthesis of $Ni^{II}(^{R}bimpy)$ Complexes

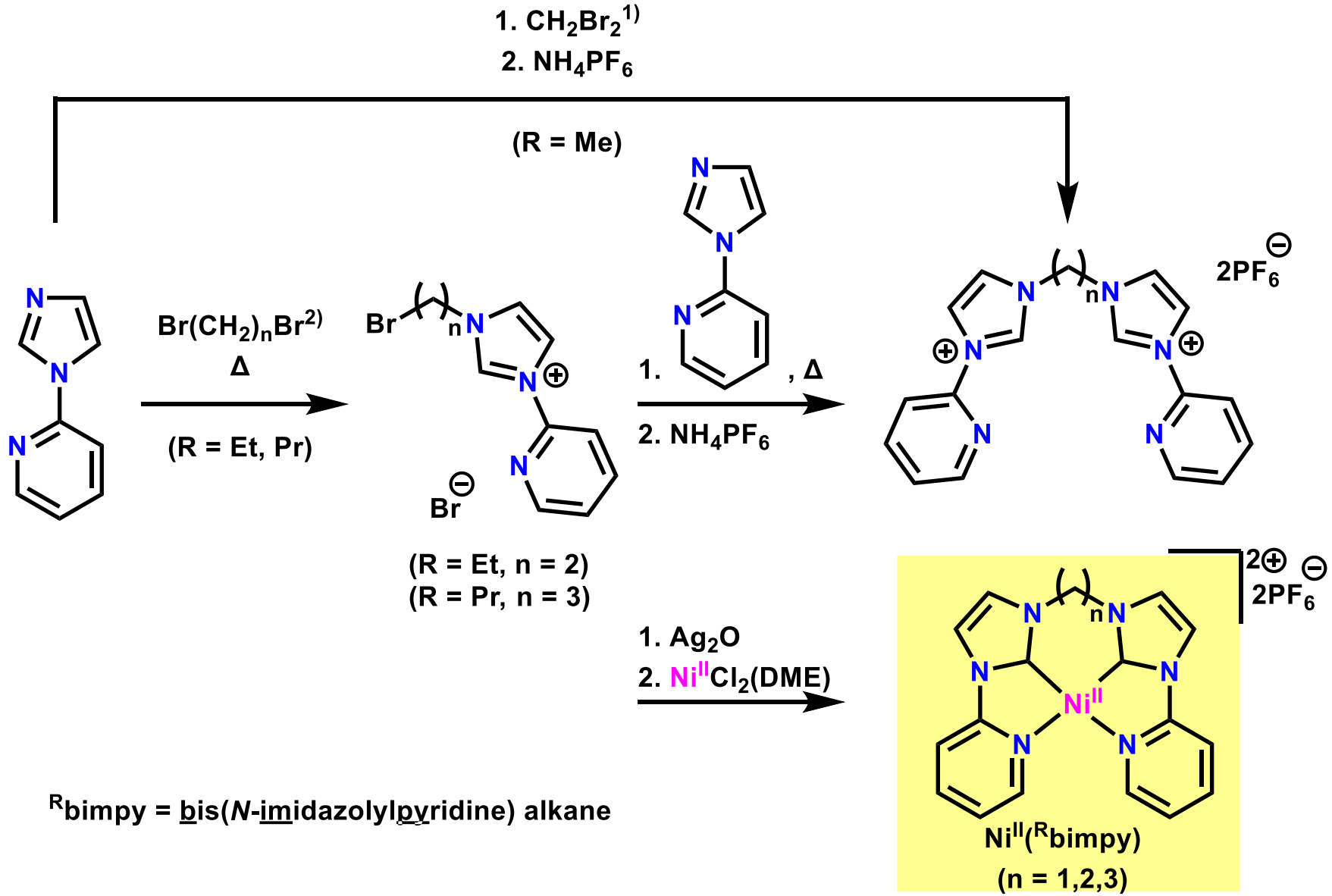

^{R}bimpy = bis(*N*-imidazolylpyridine) alkane

1) Xi, Z.; Zhang, X.; Chen, W.; Fu, S.; Wang, D. *Organometallics* **2007**, *26*, 6636.
2) Thoi, V. S.; Chang, C. J. *Chem. Commun.* **2011**, *47*, 6578.

X-Ray Structures of ^{R}bimpy Complexes

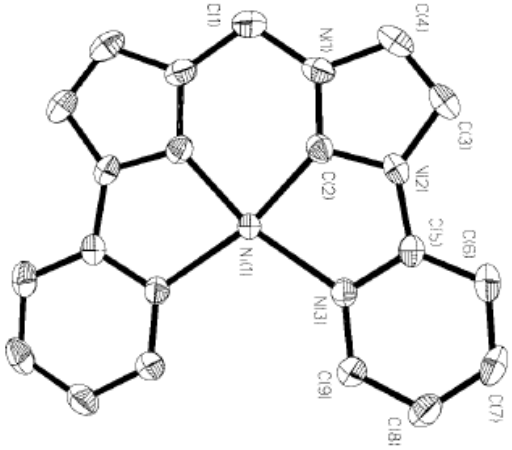

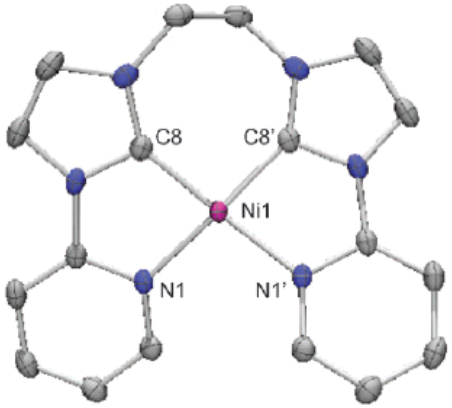

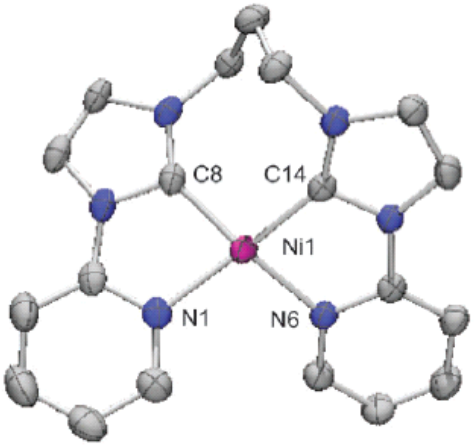

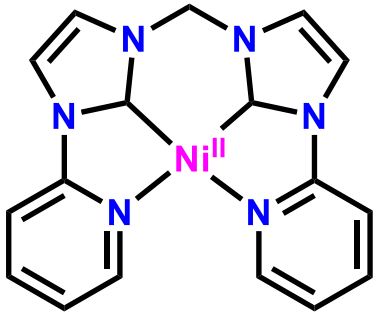

Ni^{II}(^{Me}bimpy)

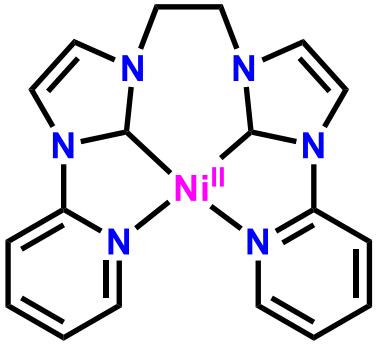

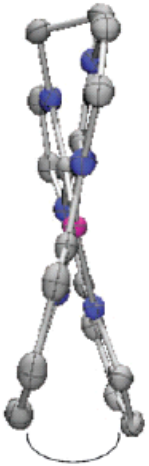

Ni^{II}(^{Et}bimpy)

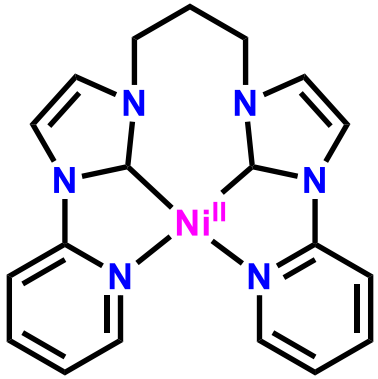

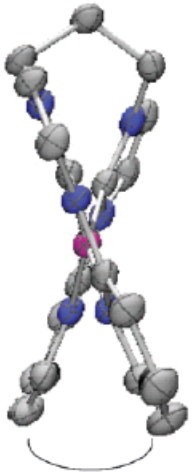

Ni^{II}(^{Pr}bimpy)

1) Xi, Z.; Zhang, X.; Chen, W.; Fu, S.; Wang, D. *Organometallics* **2007**, *26*, 6636.
2) Thoi, V. S.; Chang, C. J. *Chem. Commun.* **2011**, *47*, 6578.

Cyclic Voltammetry (CV)

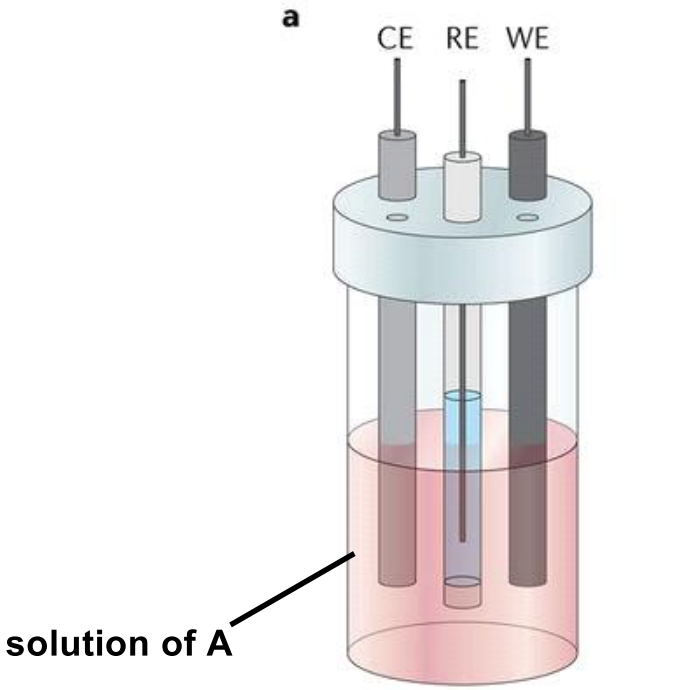

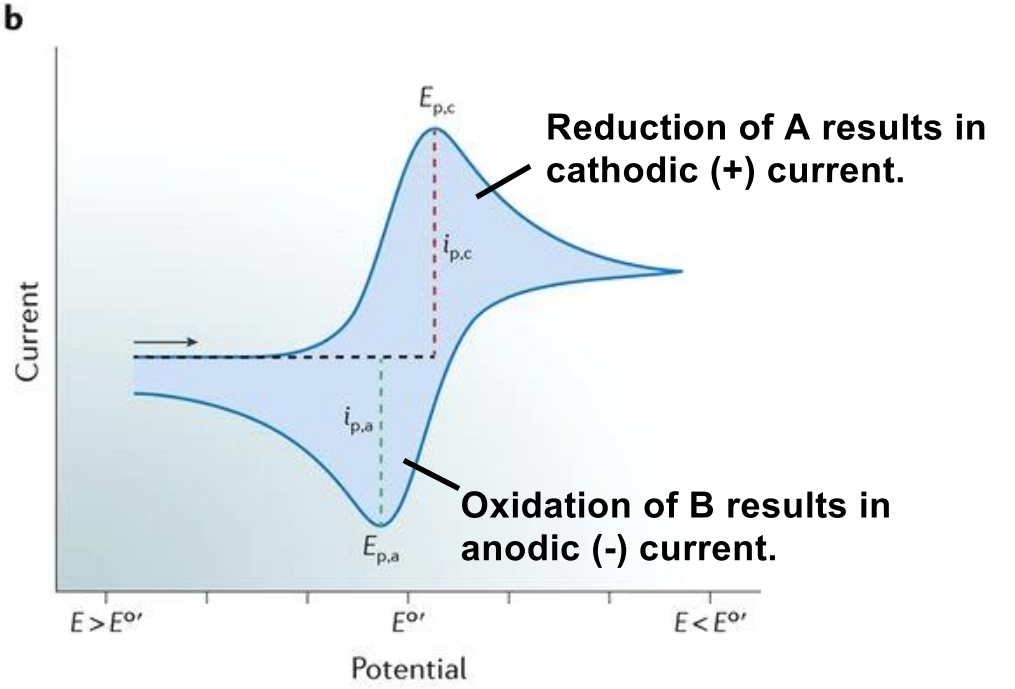

WE: working electrode
CE: counter electrode
RE: reference electrode

$E^{0\prime}$: formal reduction potential

$$A + e^- \rightleftharpoons B$$

The pair of pointsymmetric two current peaks indicates A (oxidized form) and B (reduced form) are in simple equilibrium, and there are no competing reactions. (reversible peak/wave)

When B competes in other reaction, the anodic peak attenuates or disappears due to decrease of the concentration of B. (irreversible peak)

Source of figure: Lee, K. J.; Elgrishi, N.; Kandemir, B.; Dempsey, J. L. *Nat. Rev. Chem.* **2017**, *1*, 0039.

Cyclic Voltammograms of $Ni^{II}(^{R}bimpy)$ under N_2

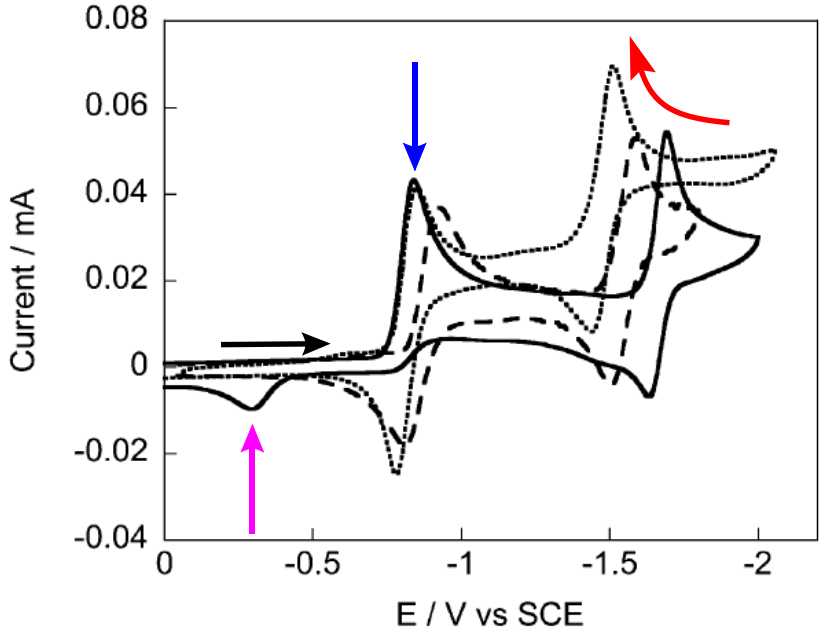

Results:
The longer alkylidene linker showed more positive potential of the second reduction.

$Ni^{II}(^{Me}bimpy)$ showed irreversible redutive peak, reversible wave and irreversible oxidative peak.

$Ni^{II}(^{Et}bimpy)$ and $Ni^{II}(^{Pr}bimpy)$ showed analogous behavior; two reversible waves.

Fig. 3 Cyclic voltammograms of complex **6** (▬▬), **7**(▬ ▬), and **8** (■■■) in 0.1 M NBu_4PF_6 in CH_3CN under a N_2 atmosphere. Scan rate: 100 mV s^{-1}; glassy carbon disk electrode. **(SCE: +0.244 V vs. SHE)**

6: $Ni^{II}(^{Me}bimpy)$
7: $Ni^{II}(^{Et}bimpy)$
8: $Ni^{II}(^{Pr}bimpy)$

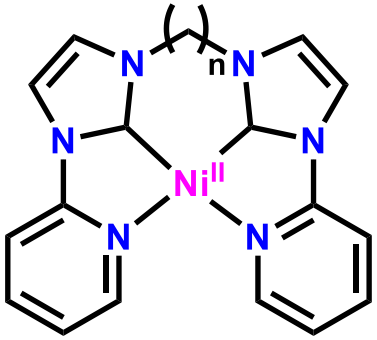

→ **Two irreversible peaks indicated the reduced $Ni^{I}(^{Me}bimpy)$ is involved in other reaction.**

Long linker allows the structural distortion of reduced complex.

Cyclic Voltammograms of $Ni^{II}(^{R}bimpy)$ under CO_2

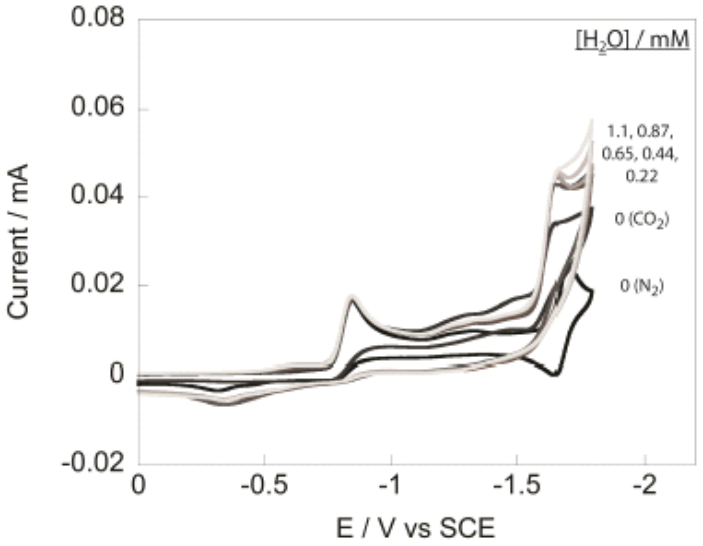

$Ni^{II}(^{Me}bimpy)$

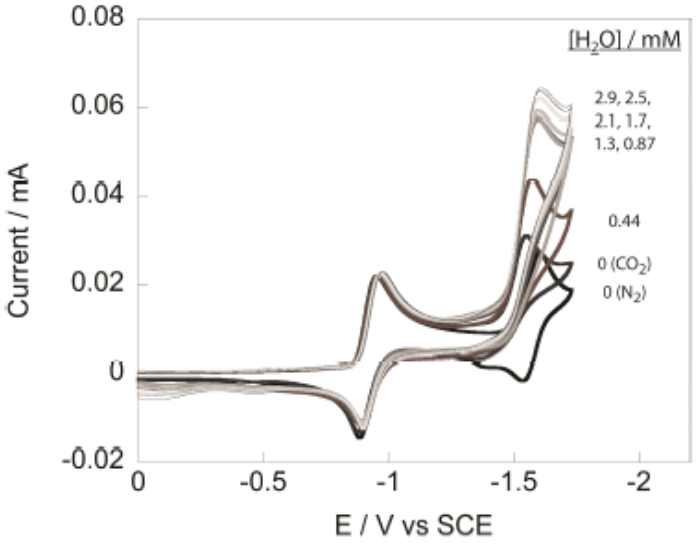

$Ni^{II}(^{Et}bimpy)$

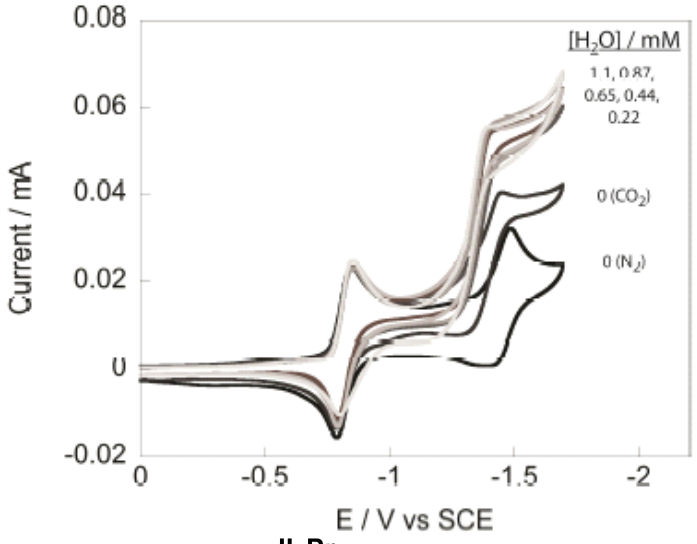

$Ni^{II}(^{Pr}bimpy)$

In each entry, current enhancement was observed when CO_2 was introduced and CO gas was detected by GC. Disappearence of oxidative peak showed that electrons are involved to reduce CO_2, not Ni^{I} complexes.

Addition of H_2O was also effective to enhance the intensity of current.

SCE: +0.244 V vs. SHE

Analysis on CO_2 Reduction by $Ni^{II}(^{Pr}bimpy)$

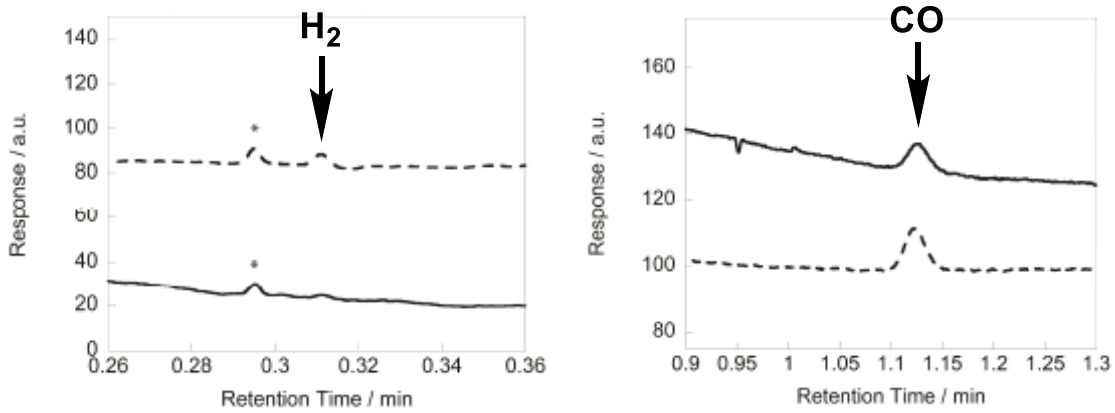

Gas chromatogram of $Ni^{II}(^{Pr}bimpy)$ after 2 h electrolysis at -1.3 V (vs. SHE) in 0.3 M Bu_4NPF_6 in wet CH_3CN, using a glassy carbon rod electrode.

——— without addition of H_2

- - - - - - with addition of 10 uL H_2 before GC analysis

*unknown trace component also observed in a blank sample of air

$Ni^{II}(^{R}bimpy)$	applied potential*	TOF (turnover frequencies)
$Ni^{II}(^{Me}bimpy)$	-1.5 V	3.9 h^{-1}
$Ni^{II}(^{Et}bimpy)$	-1.4 V	4.2 h^{-1}
$Ni^{II}(^{Pr}bimpy)$	-1.3 V	5.9 h^{-1}

*** vs. SHE.**

Only trace amount of H_2 was produced during the electrocatalysis.

$Ni^{II}(^{R}bimpy)$ showed high selectivity for activating CO_2 over H_2O under this electrocatalytic conditions.
But its activity was very modest, and continuous electrolysis at high cathodic potentials led to catalyst deactivation.

Plausible Catalytic Cycle of CO_2 Reduction

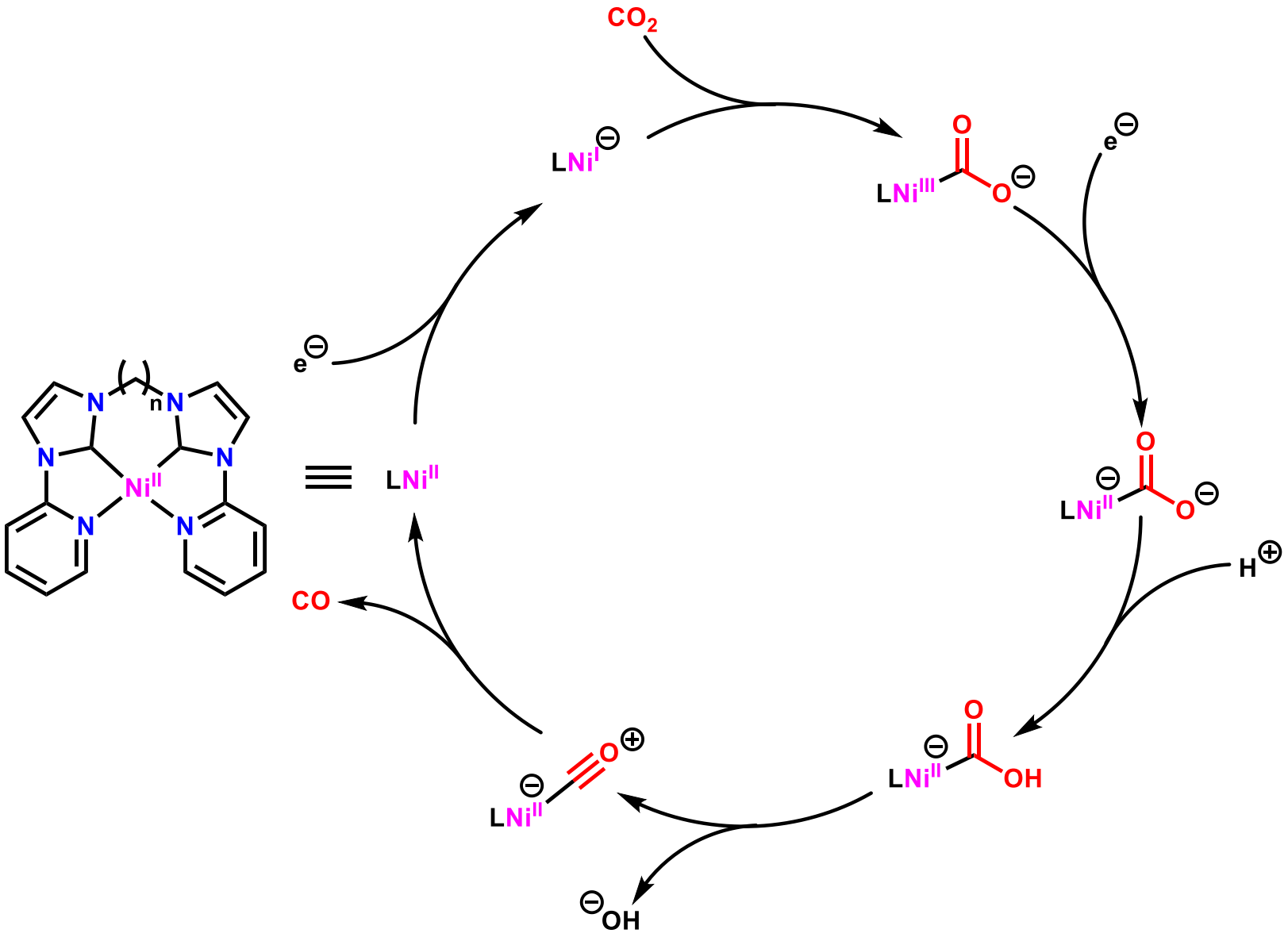

Leung, K.; Nielsen, I, M.; Sai, N.; Medforth, C.; Shelnutt, J. A.; *J. Phys. Chem. A* **2010**, *114*, 10174.

Short Summary

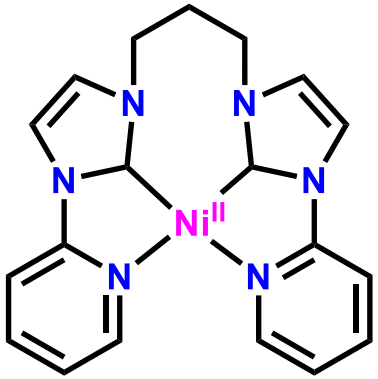

CO_2 → CO

glassy carbon electrode

Bu_4NPF_6, wet CH_3CN

-1.3 V (vs. SHE)

TOF: 5.9 h^{-1}

Improvement

- New homologous catalyst for electronic reduction of CO_2 without Hg electrode.
- High selectivity for CO_2 reduction over H_2O.
- Structural modification of ligand could change the reduction potential systematically.

But...

- Modest activity
- Highly cathodic potential
- Instability under electrocatalytic condition
- Incompatibility with pure aqueous media?

Contents

1. Electrocatalytic reduction of CO_2 using nickel complexes in organic media (Chang, 2011)
   Chem. Commun. **2011**, *47*, 6578.

2. Electrocatalytic reduction of CO_2 on covalent organic frameworks (COFs) in water
   (Yaghi and Chang, 2015 and 2017)
   Science **2015**, *349*, 1208.
   J. Am. Chem. Soc. **2018**, *140*, 1116.

Omar M. Yaghi

1985 B.S. State University of New York at Albany
1990 Ph.D. University of Illinois-Urbana
(Prof. W. G. Klemperer, metal polyoxoanions)
1990-1992 Postdoc Harvard University
(Prof. R. H. Holm, metal polyoxoanions)
1992-1999 Assistant Prof., Arizona state University
1999-2006 Prof., University of Michigan
2006-2012 Prof., UCLA
2012-present Prof. UC Berkeley

Research topics:
Metal-organic frameworks (MOFs)
Covalent organic frameworks (COFs)
Zeolitic imidazolate frameworks (ZIFs)
Metal-organic polyhedra
New porous crystals

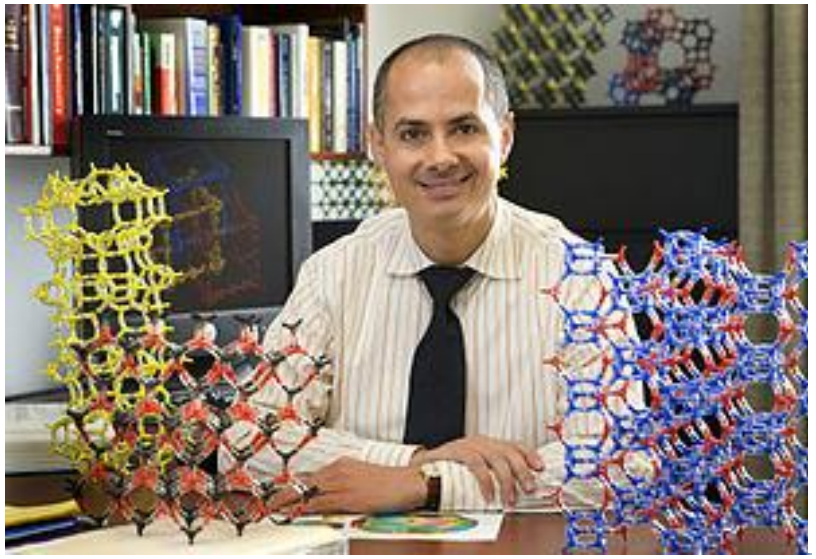

Covalent Organic Frameworks (COFs)

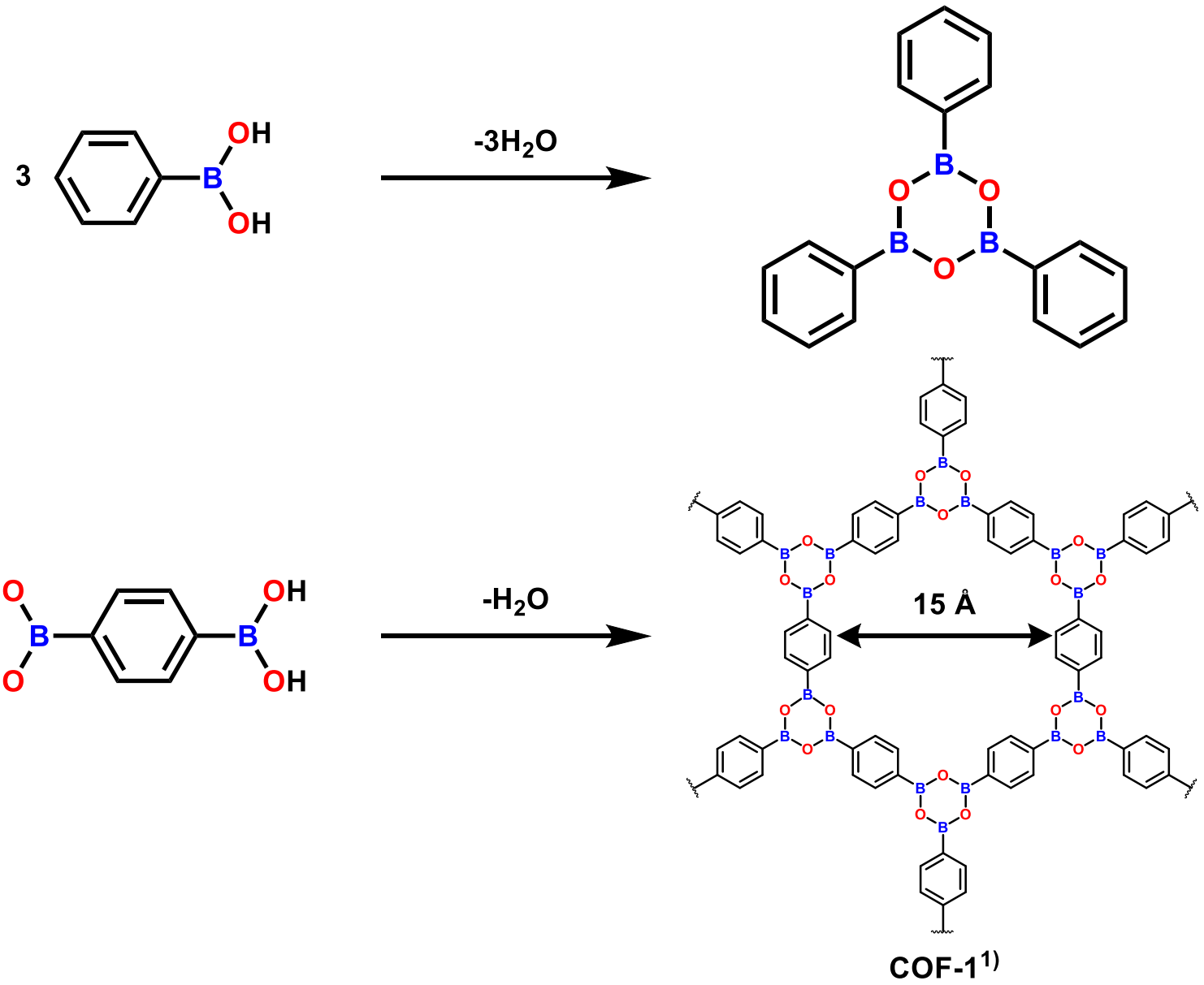

1) Côté, A. P.; Benin, A. I.; Ockwig, N. W.; O'Keeffe, M.; Matzger, A. J.; Yaghi, O. M. *Science* **2005**, *310*, 1166.

Differnce from Metal Organic Frameworks (MOFs)

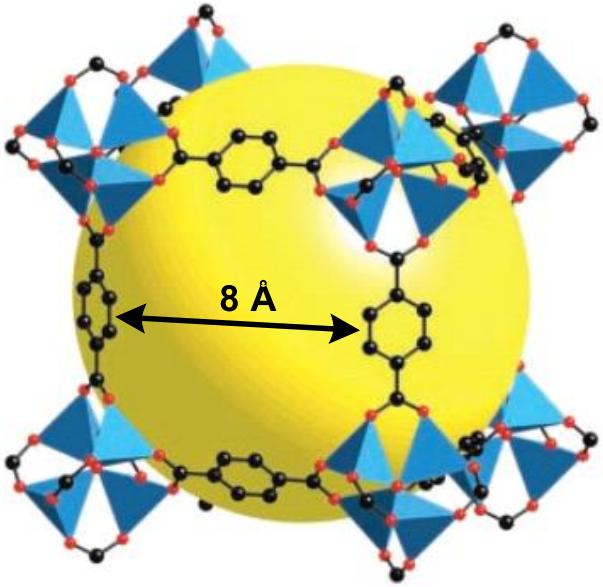

blue: tetra-coordinated Zn
red: O, black: C
yellow: 12 Å-diameter pore

MOF-5[2)]

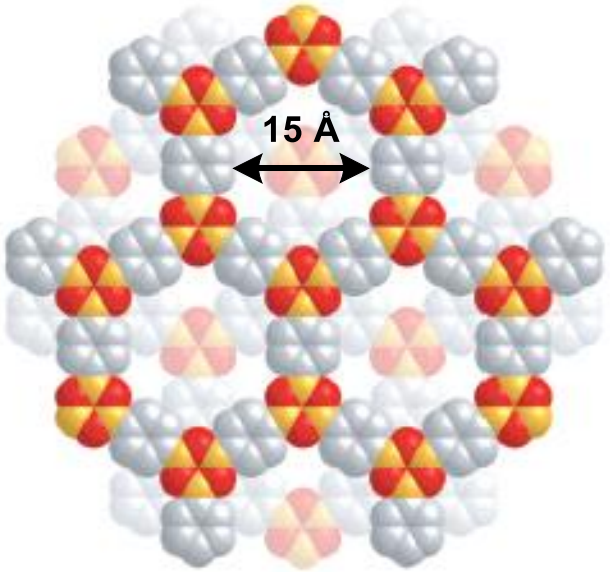

COF-1[1)]

Common feature

- porous crystalline compound
- high surface area
- tunable pore size
- thermal stability
- stability in water

Differnce

MOFs

- consist of metal oxide and linking organic component
- linked by coordination or ionic bond

COFs

- consist of only light elements (B, C, N, O, H)
- linked by covalent bond

1) Côté, A. P.; Benin, A. I.; Ockwig, N. W.; O'Keeffe, M.; Matzger, A. J.; Yaghi, O. M. *Science* **2005**, *310*, 1166.
2) Rosi, N. L.; Eckert, J.; Eddaoudi, M.; Vodak, D. T.; Kim, J.; O'Keeffe, M.; Yaghi, O. M. *Science* **2003**, *300*, 1127.

New Strategy with COF

Homogeneous catalyst (such as $Ni^{II}(^{R}bimpy)$)

- requires organic media for selectivity, stability and solubility
- relatively easy to optimize

Heterogeneous catalyst

- often stable in water
- difficult to optimize

COFs

- tunability with various building blocks
- established strategy to design the topological structure

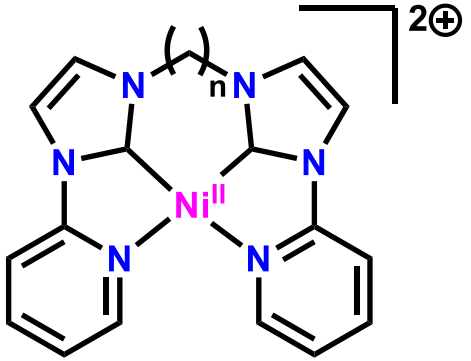

$Ni^{II}(^{R}bimpy)$

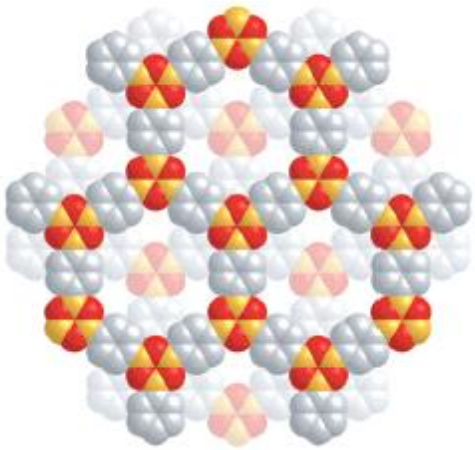

→ **Use of COFs as a platform can open up a new strategy of electrocatalysis.**

Synthesis of Catalyst-Containing COFs

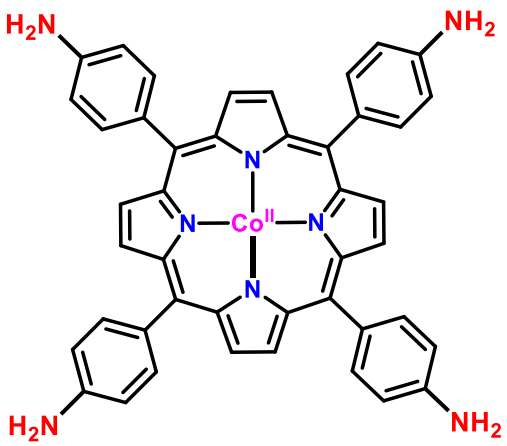

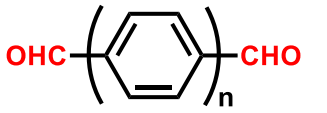

1,2-dichlorobenzene
BuOH, AcOH aq.
0.05 mmHg, 120 °C

92% (COF-366-Co)
63% (COF-367-Co)

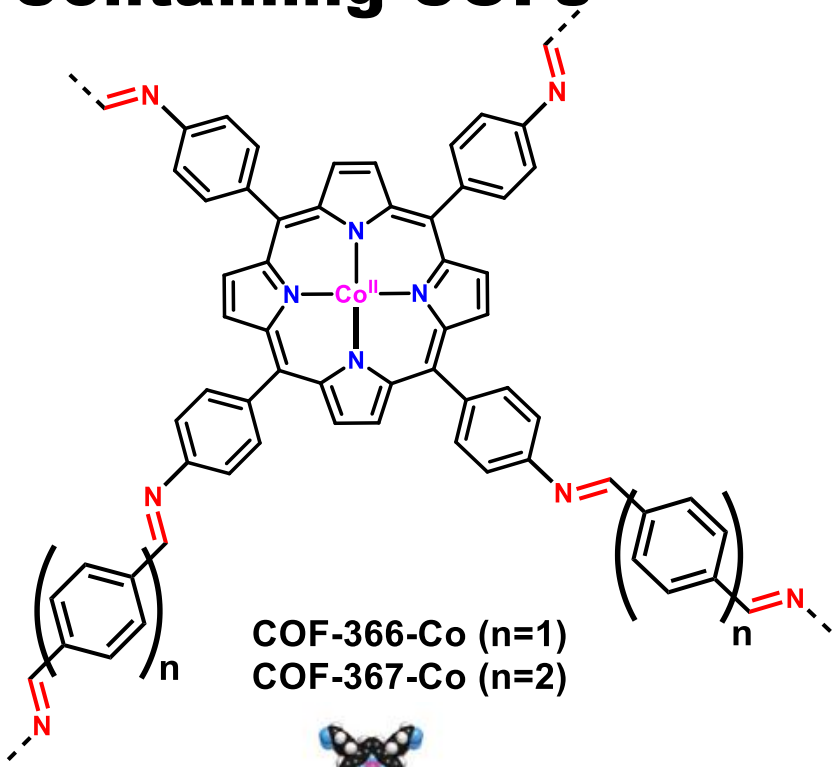

COF-366-Co (n=1)
COF-367-Co (n=2)

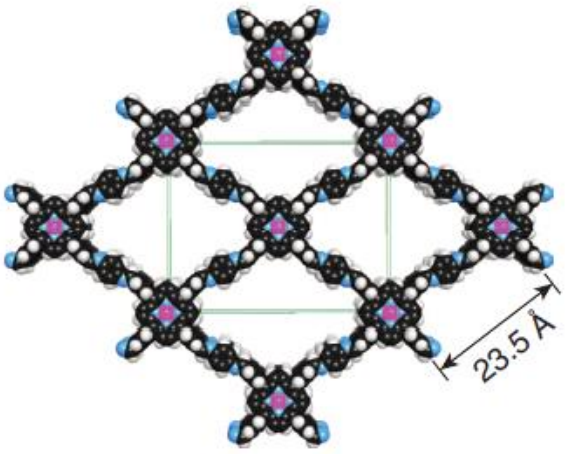

COF-366-Co

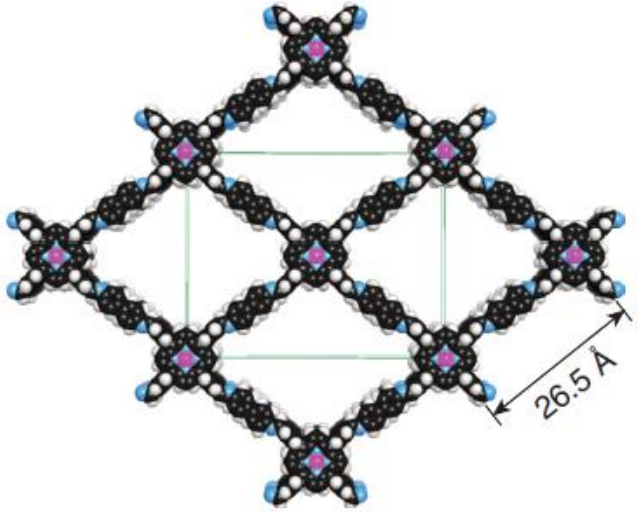

COF-367-Co

Structure Elucidation of the Framework

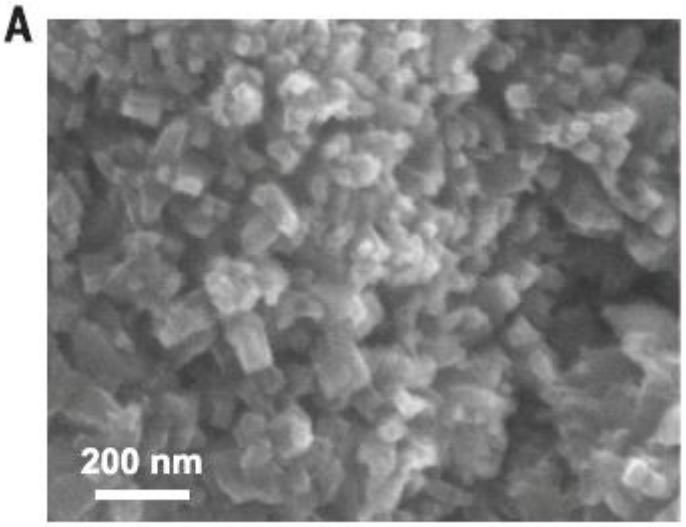

SEM (Scanning Electron Microscopy)
image of COF-366-Co sample

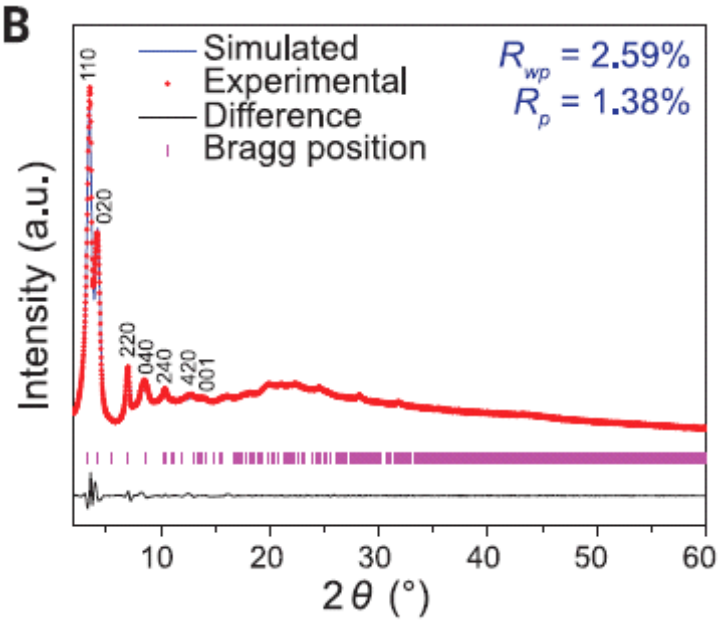

PXRD (Powder X-Ray Diffraction)
patterns of COF-366-Co

one kind of morphology
(~50 nm in length)

Pawley refinement:
profile fitting against simulated model
R_{wp}: weighted-profile reliability factor
R_p: unweighted-profile reliability factor

good agreement with proposed model
1D channel (width: 21 Å)
stacking 2D sheets (distance: 4.4 Å)

Structure Elucidation of the Framework

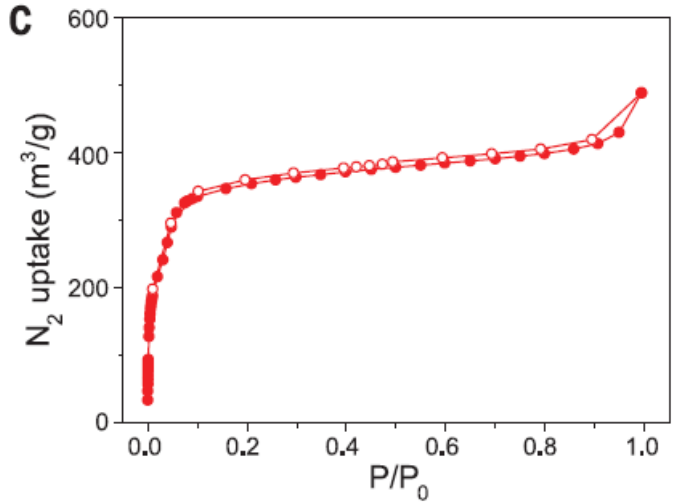

N_2 adsorption isotherms of COF-366-Co at 77 K
P: pressure of the system
P_0: saturartion pressure of N_2 at 77 K

The shape of adsorption isotherms differs dependently on the state of adsorbent surface: presence of pore, size of pore and interaction with adsorbate.

Isotherm of COF-366-Co showed

- microporous structure
- narrow pore size distribution between 10-18 Å
- BET surface area is 1360 m^2/g

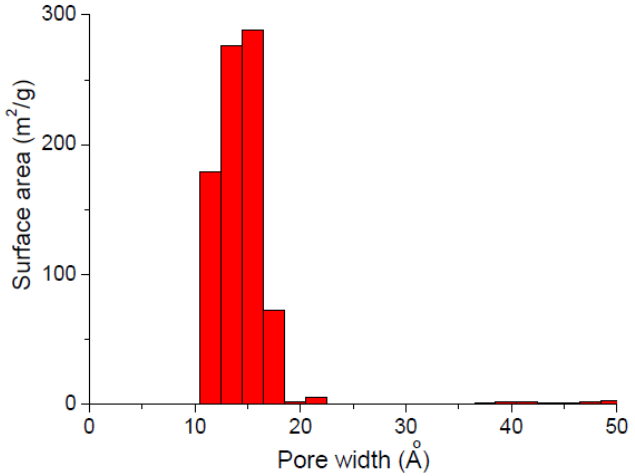

pore size distribution of COF-366-Co calculated from DFT-fitting of N_2 adsorption isotherm

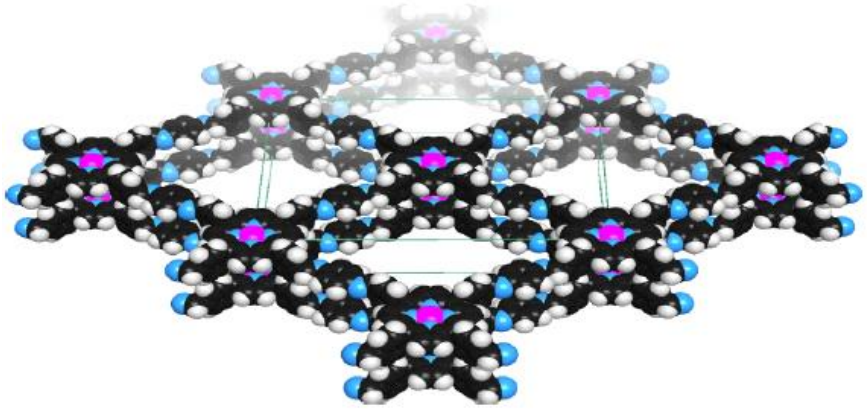

Cyclic Voltammogram of COF-366/367-Co

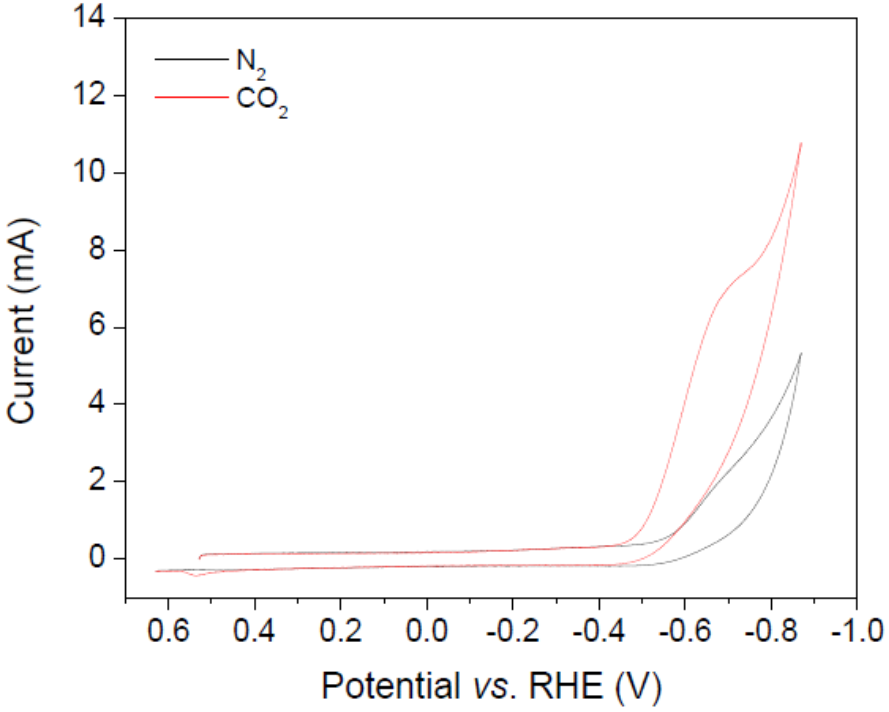

COF-366-Co

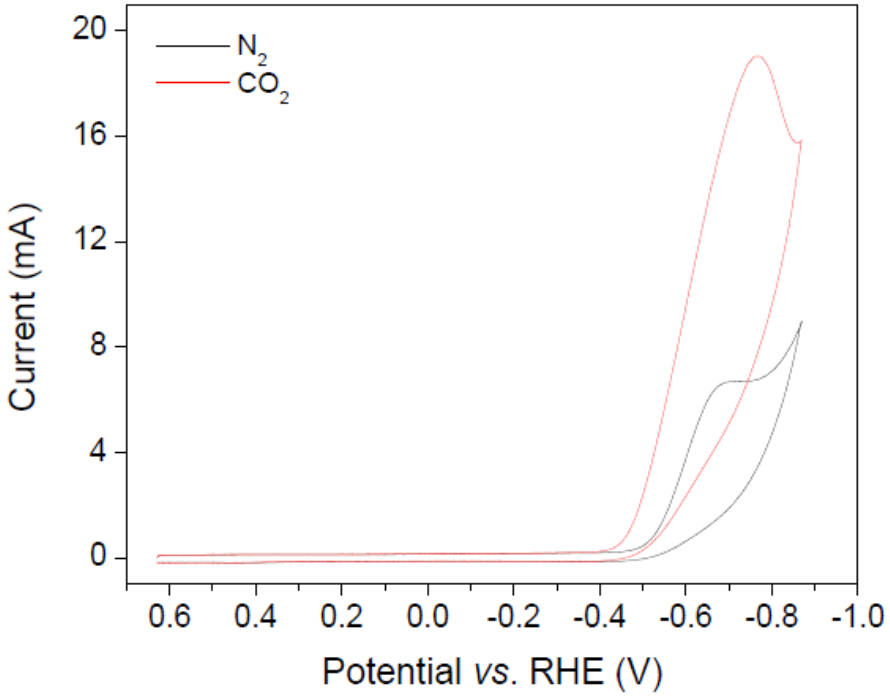

COF-367-Co

pH = 7.2
RHE: -0.42 V vs. SHE (at pH = 7.2)

	pore size distribution	surface area
COF-366-Co (phenylene linker)	10-18 Å	1360 m^2/g
COF-367-Co (biphenyl linker)	12-23 Å	1470 m^2/g

In both cyclic voltammogram, significant enhancement of current was observed when the sample solution was saturated with CO_2.

→ **Extra current was caused by reductive reaction on the electrode.**

Electrolyses with Deposited COFs

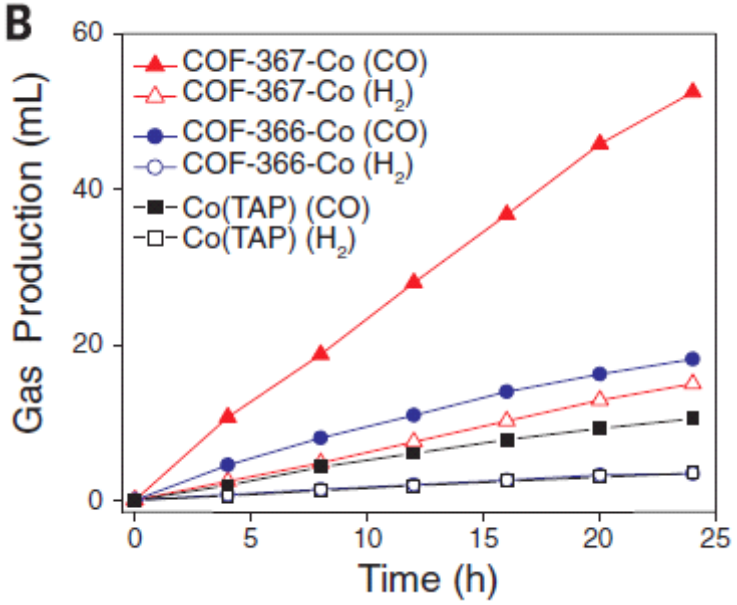

Electrolysis at -1.10 V (vs. SHE)
in $KHCO_3$ aq. pH = 7.3

	TON	TOF	Current Efficiency
Co(TAP) (building block)	794	36 h^{-1}	80%
COF-366-Co (phenylene linker)	1352	98 h^{-1}	90%
COF-367-Co (biphenyl linker)	3901	165 h^{-1}	91%

selectivity for CO_2 reduction over H_2O in aqueous media
high activity on CO_2 reduction
high current efficiency
long-term stability

→ But, not all the Co atoms on COFs were involved in the reduction presumably due to the limited electrochemical contact between the deposited COF powder and the electrode.

Direct Growing of COF-366-Co onto Electrode

COF was directly grown on highly ordered pyrolytic graphite (HOPG), a kind of artificial graphite with high purity and ordered surface.

Crystallinity and orientation of growth were confirmed by X-ray experiment (grazing incidence wide-angle X-ray scattering, GIWAXS).

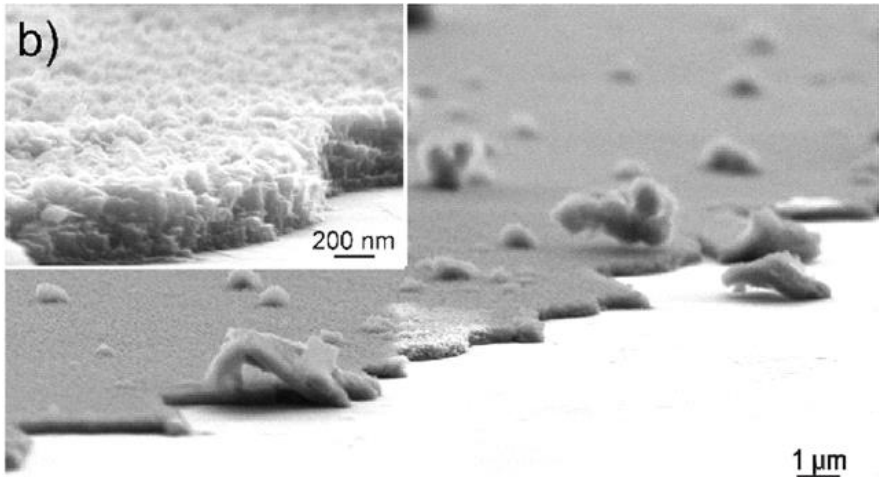

SEM image of uniform COF films (~250 nm in thickness) on HOPG.

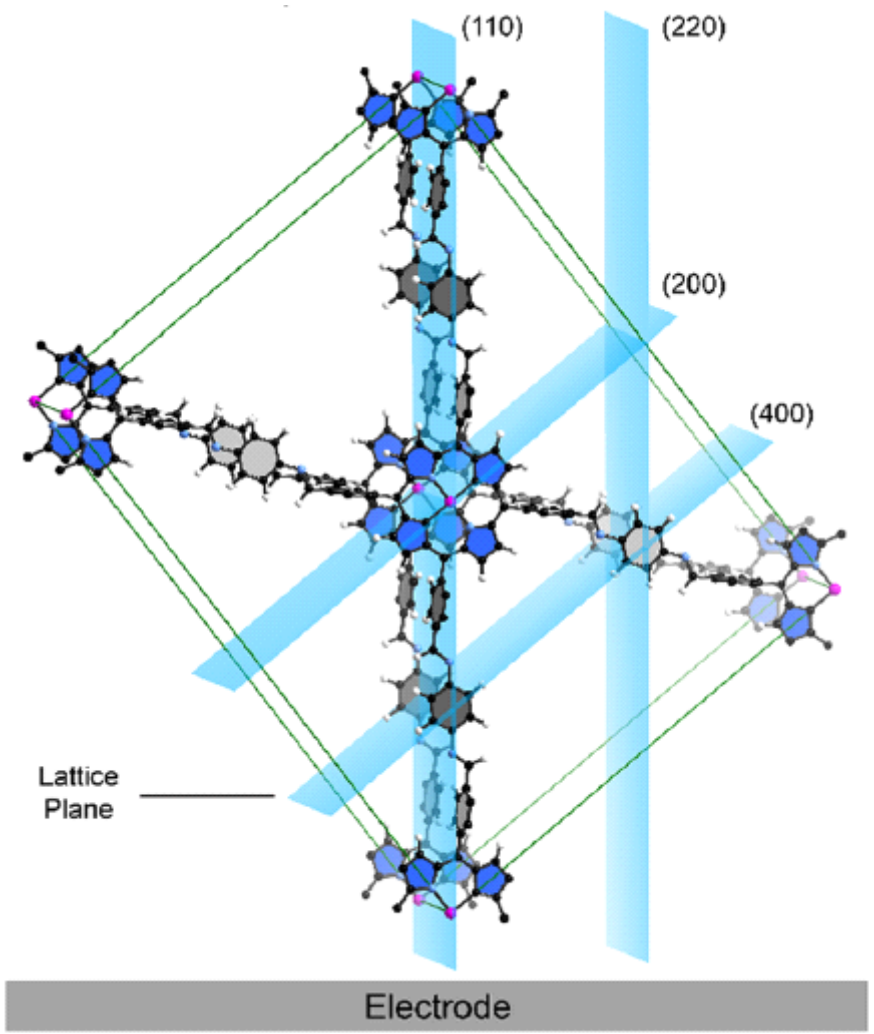

3D structure of COF-366-Co directly grown onto HOPG suggested by GIWAXS experiment. COF grew perpendicularly to graphite surface.

Electrolysis Using Oriented COF

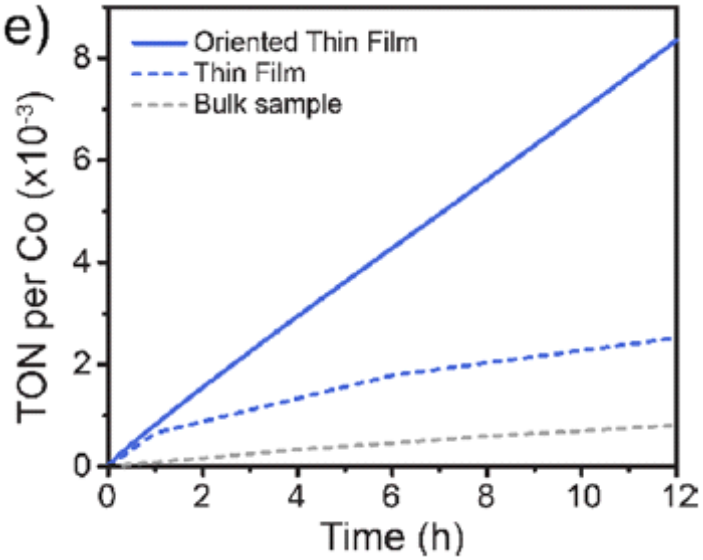

oriented film on HOPG

unoriented film on glassy carbon

deposited powders on glassy carbon

Electrolyses with various states of COF-366-Co.
$KHCO_3$ aq., pH = 7.2, -1.10 V (vs. SHE)

- **Significant enhancement of electrocatalytic activity** was observed. (vs. deposited powder)
- **Long-term stability** was brought by proper orientation of COF film. (vs. COF on glassy carbon)

→ Optimization of crystal morphology was accomplished.

Next: Can reactivity of the catalyst be tuned by structural modification?

Functionalization of COFs

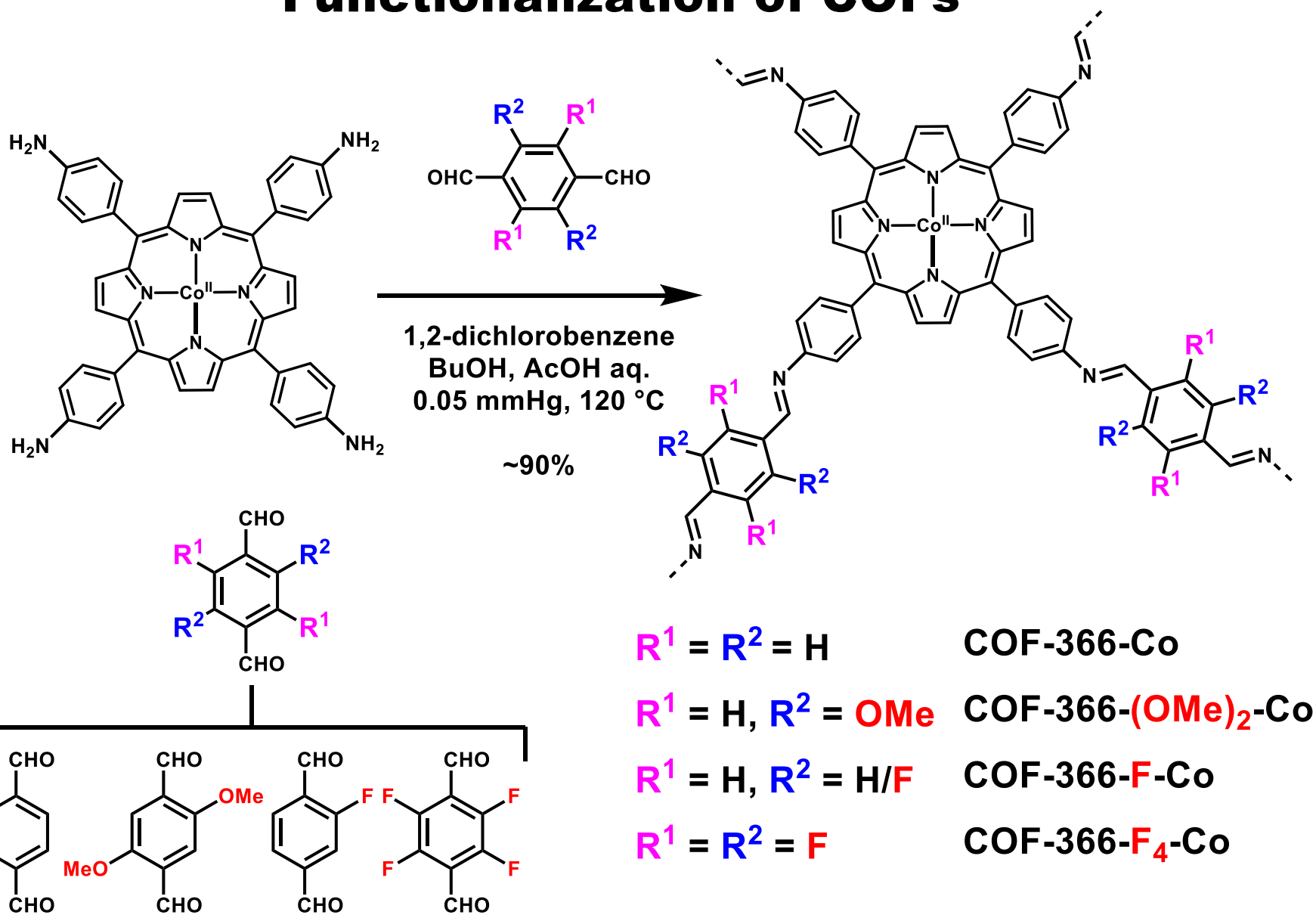

Property of the COFs: Electronic Structure of Co

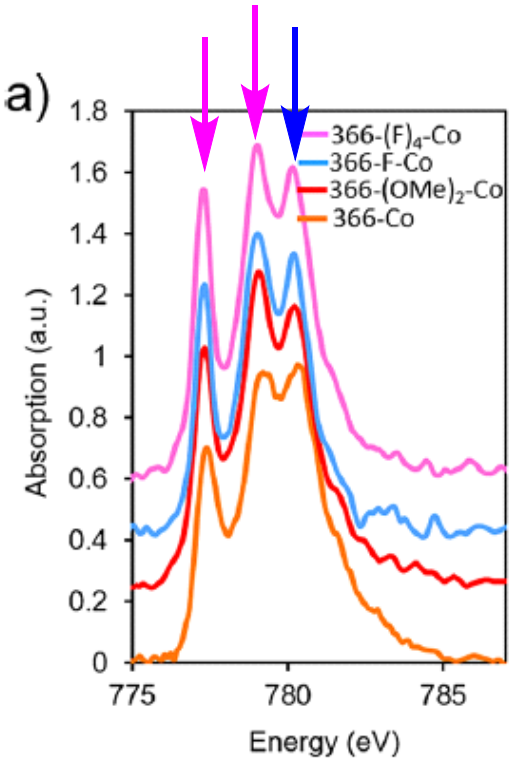

XAS Co L-edge spectra of COFs.

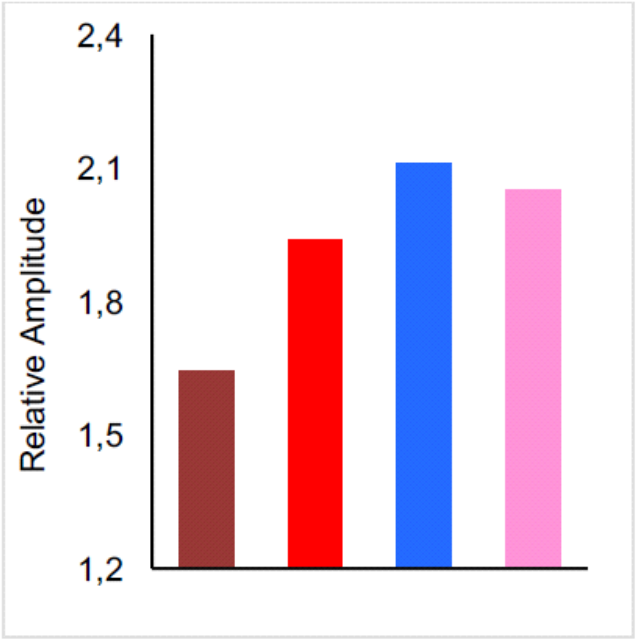

$(I_{777}+I_{779})/I_{780}$
brown: 366-Co; red: 366-$(OMe)_2$-Co;
blue: 366-F-Co; pink: 366-F_4-Co.

X-ray absorption spectroscopy (XAS)

Obtained peaks called "L-edge" feature the electron transition from 2p orbital to unoccupied 3d.
Resulting spectrum reflects the electronic state of the probed element.

It was confirmed in control experiment that intensity of peaks at 777 and 779 eV enhances with increasing electron withdrawing character of ligands.
Authors evaluated the effect of substituents with relative intensity at 777 and 779 eV (I_{777}, I_{779}) against that at 780 eV (I_{780}).

Cyclic Voltammograms of Substituted COFs

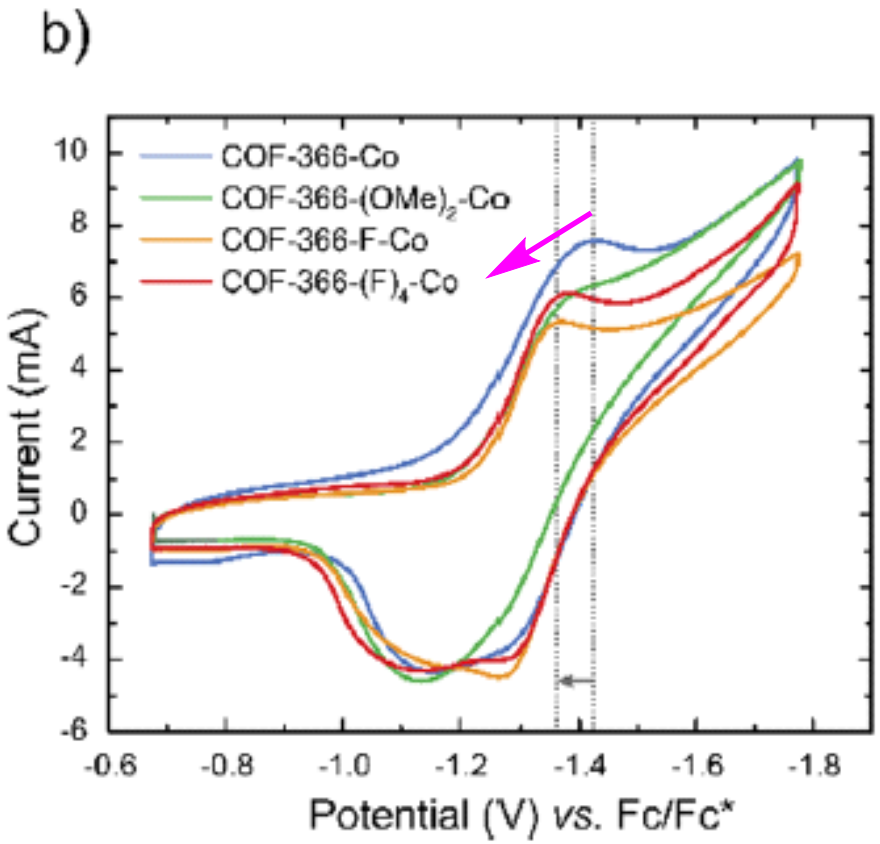

E^0_{Fc/Fc^*} : +0.38 V (vs. SHE)

Shift of cathodic peak was observed as the electron density of Co decreased.

366-F-Co (-1.00 V vs. SHE) > 366-F_4-Co ~ 366-$(OMe)_2$-Co > 366-Co (-1.05 V vs. SHE)

Electrolysis with Substituted COFs

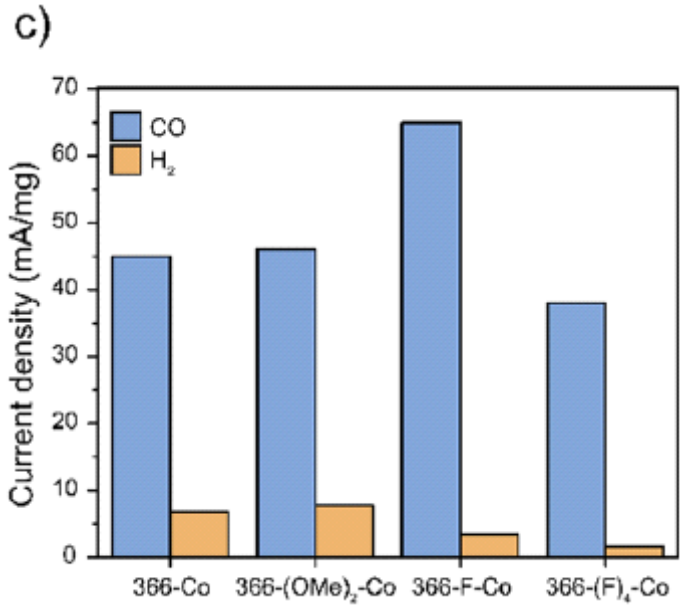

Current density (per mg of Co) under electrolysis at -1.10 V (vs. SHE) in 0.5 M $KHCO_3$ aq (pH = 7.3).

366-F-Co, the most electron-deficient COF, showed best current density. (Current density means how much amount of electrons transferred by unit amount of Co atoms in unit time.)

Authors reasoned low activity of 366-F_4-Co was due to the higher hydrophobicity which resulted decreased access of electrolyte (H_2O, H_3O^+, ...) to the catalytic center.

Summary

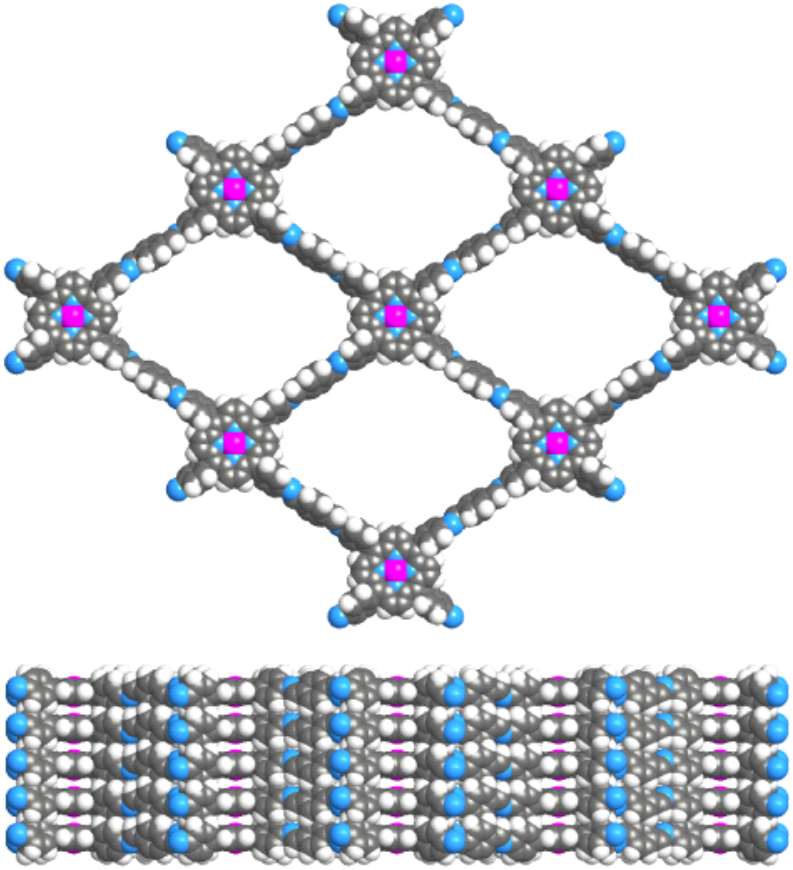

From a view of electrocatalysis:
- Effective electrolysis in aqueous media
- Relatively low potential
- High selectivity over H_2O
- No use of rare/toxic metals
- Stability through long-term use

From a view of organic/material chemistry:
- Electronic tunability on heterogeneous frameworks
- Controlled morphology of supramolecule

Future perspective (including my opinion):
- More systematic tuning of metal center
- Active site on linker
- Catalyst on 3D COFs

Appendix

$Ni^{II}(^{Me}bimpy)$ in Suzuki-Miyaura Coupling

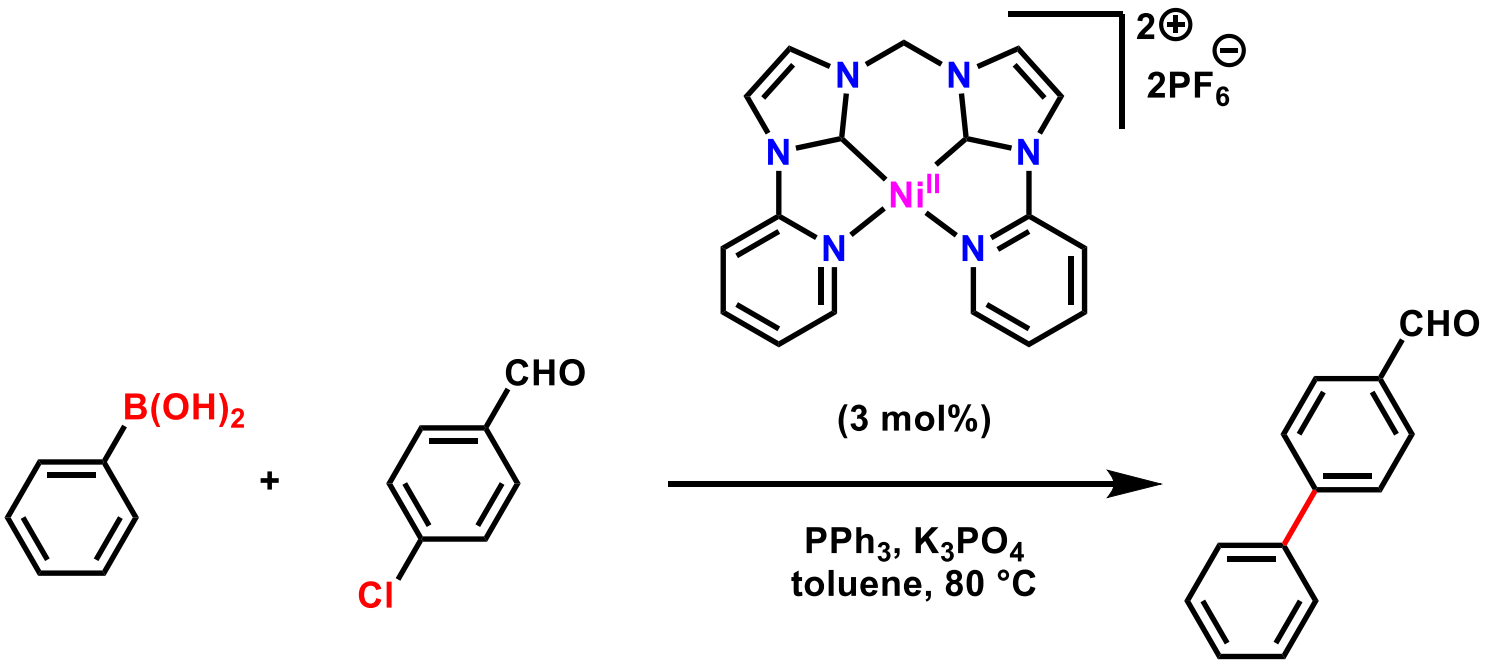

Chemical Reduction of $Ni^{II}(^{Me}bimpy)$

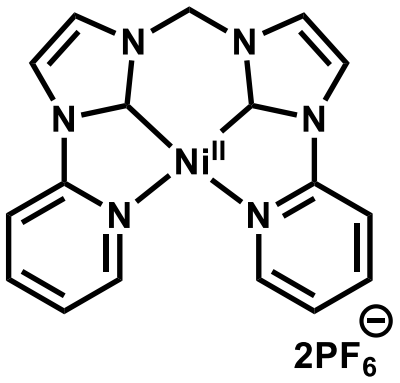

KC_8

THF

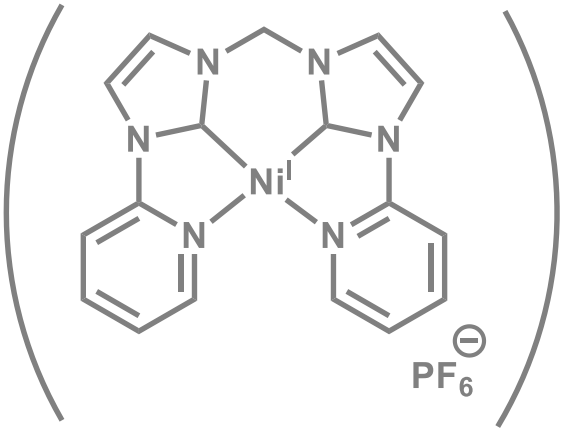

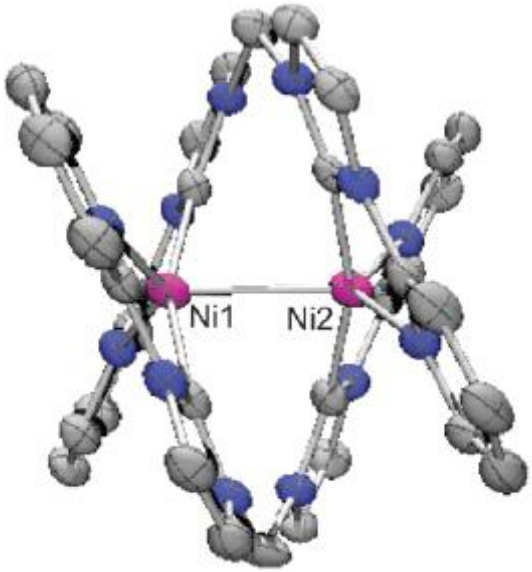

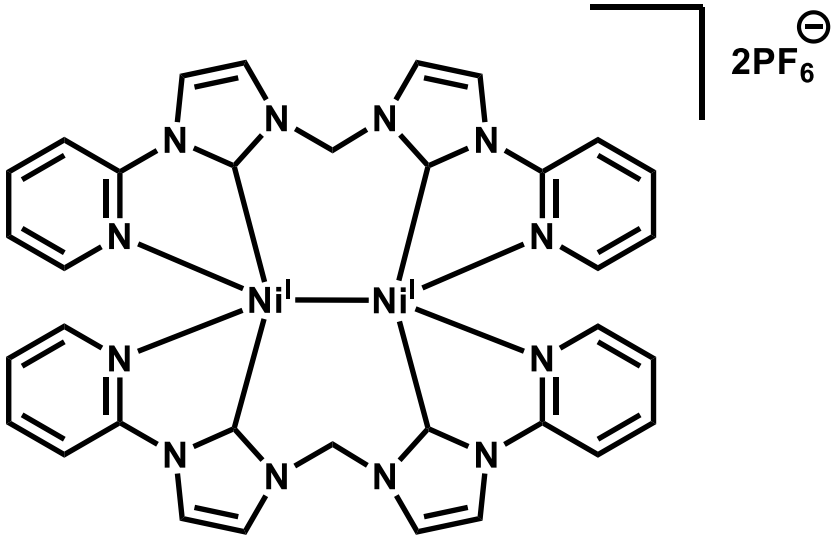

→ Reduction of $Ni^{II}(^{Me}bimpy)$ causes dimerization.
Square planar structure of Ni^{I} might be unfavored.

CV of $Ni^{II}(^{R}bimpy)$ under N_2 with H_2O

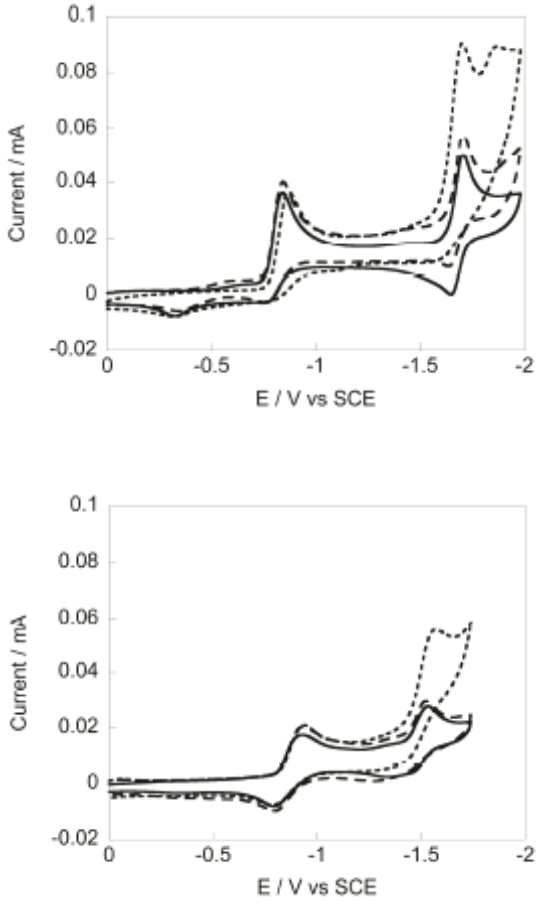

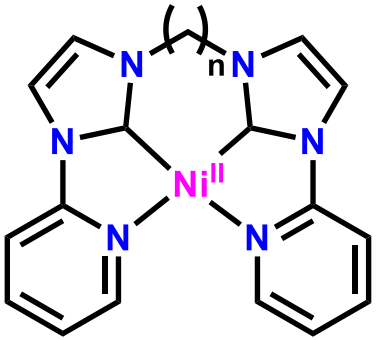

6: $Ni^{II}(^{Me}bimpy)$

7: $Ni^{II}(^{Et}bimpy)$

Fig. S3 Cyclic voltammograms of **6** (top) and **7** (bottom) in the presence of N_2 (▬), 0.87 mM H_2O under a N_2 atmosphere (▬ ▬), and subsequently, 0.87 mM H_2O under a CO_2 atmosphere (▪▪▪) in 0.1 M NBu_4PF_6 in CH_3CN. Scan rate: 100 mV/s; glassy carbon disk electrode.

CV of ^{R}bimpy ligand under N_2 and CO_2

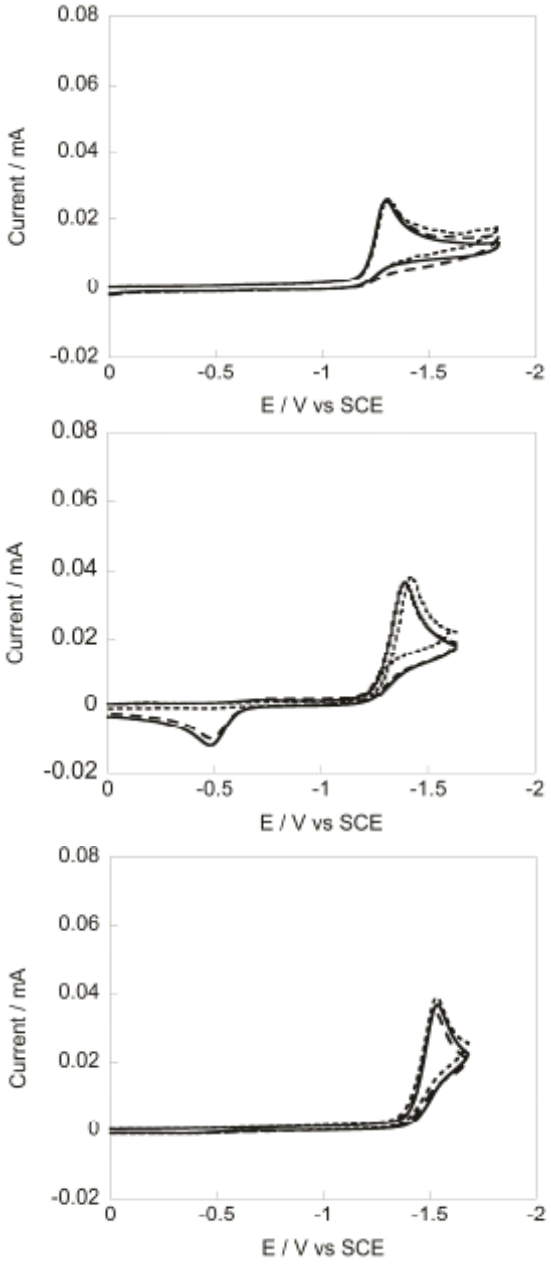

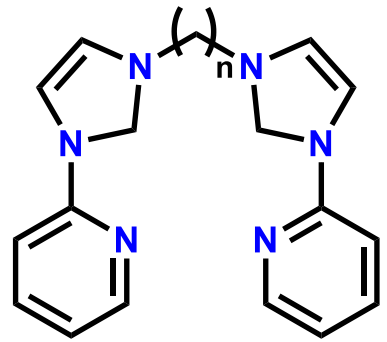

3: ^{Me}**bimpy**
4: ^{Et}**bimpy**
5: ^{Pr}**bimpy**

Fig. S4 Cyclic voltammograms of **3** (top), **4** (middle), and **5** (bottom) in the presence of N_2 (▬), CO_2 (▬ ▬), and subsequently, 0.44 mM H_2O under a CO_2 atmosphere (▬) in 0.1 M NBu_4PF_6 in CH_3CN. Scan rate: 100 mV/s; glassy carbon disk electrode.

Control Experiment on XAS

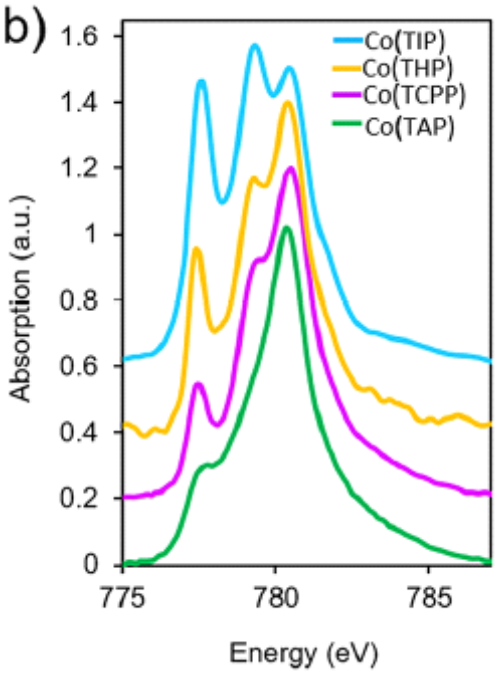

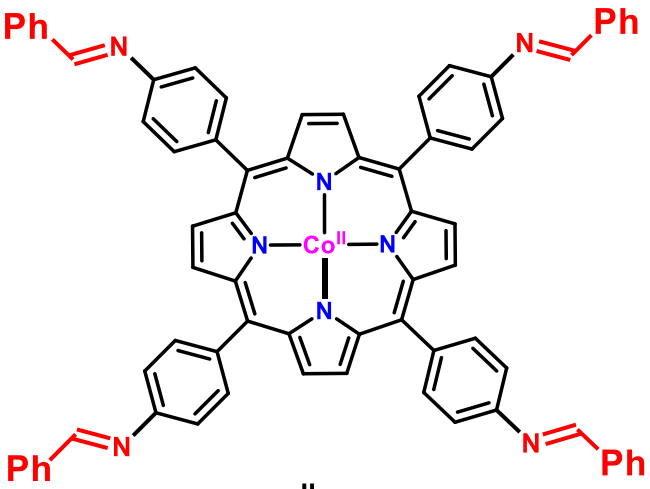

Co^{II}(TIP)

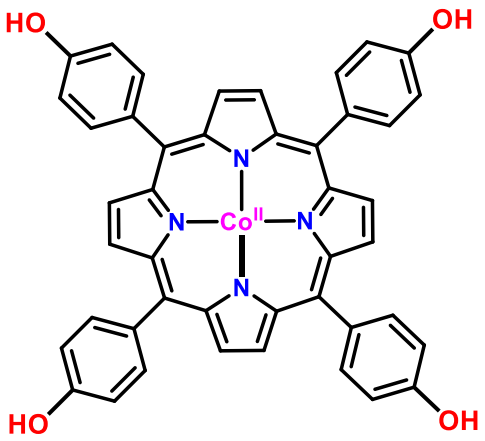

Co^{II}(THP)

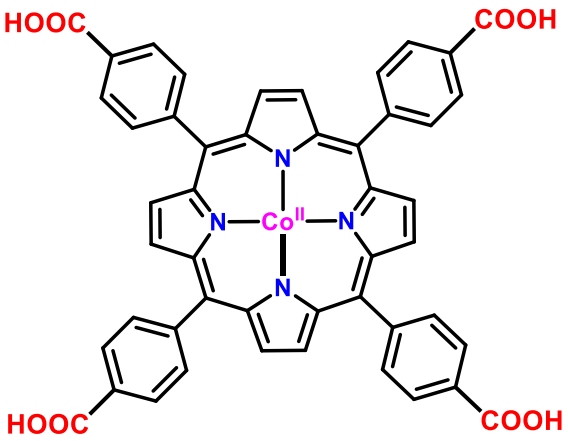

Co^{II}(TCPP)

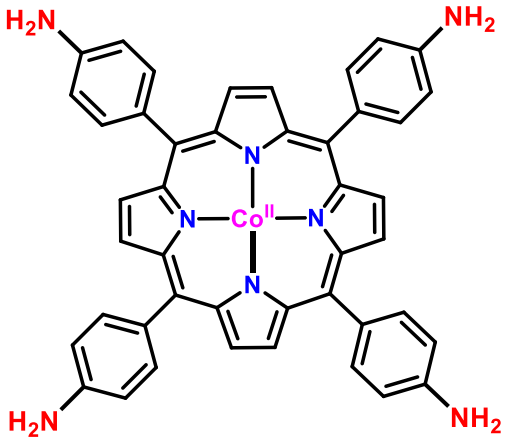

Co^{II}(TAP)

CO_2 Uptake of Substituted COFs

Table 1. Pore Size Distribution (PSD), BET Surface Area (A_{BET}), CO_2 Uptake, and Isosteric Heat of Adsorption (Q_{st}) Values for the Binding of CO_2 for the COF Catalysts

material	PSD (Å)[a]	A_{BET} ($m^2\ g^{-1}$)[b]	CO_2 uptake ($cm^3\ g^{-1}$)[c]	Q_{st} (kJ mol^{-1})[d]
COF-366-Co	10–18	1700	23.4	24.6
COF-366-$(OMe)_2$-Co	8–18	867	24.2	24.4
COF-366–F-Co	10–18	1901	27.0	24.2
COF-366-$(F)_4$-Co	8–16	832	27.4	24.1

[a]Determined by fitting of the adsorption branch using quenched solid state density functional theory (QSDFT) cylindrical/slit pore model on the absorption branch of the isotherm. [b]Calculated using the BET method from the nitrogen sorption data of the activated samples at 77 K. [c]Uptake at 800 Torr and 298 K, the conditions under which we carry out the catalysis. [d]Calculated from pure component isotherms using Henry's law.

Determination of Applying Potential

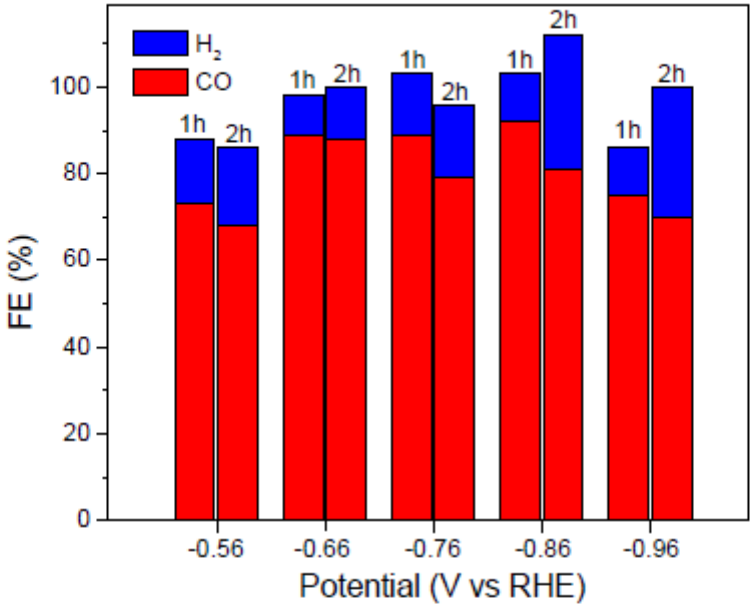

Figure S64. Faradaic efficiency of COF-366-Co catalzyed CO_2 reduction as a function of applied potential. The graph shows that potentials less negative than -0.66 V are ideal for COF-366-Co catalyzed CO_2 reduction in terms of the stability of the material. At potentials higher than -0.76 V, a significant decrease of rate of CO evolution is observed in the 2nd-hour electrolysis compared to the 1st-hour, which is accompanied by an increase of the amount H_2 produced. This observation indicates the decomposition, presumably through demetallation of the porphyrin sites, during electrolysis under these potentials.

3D COFs

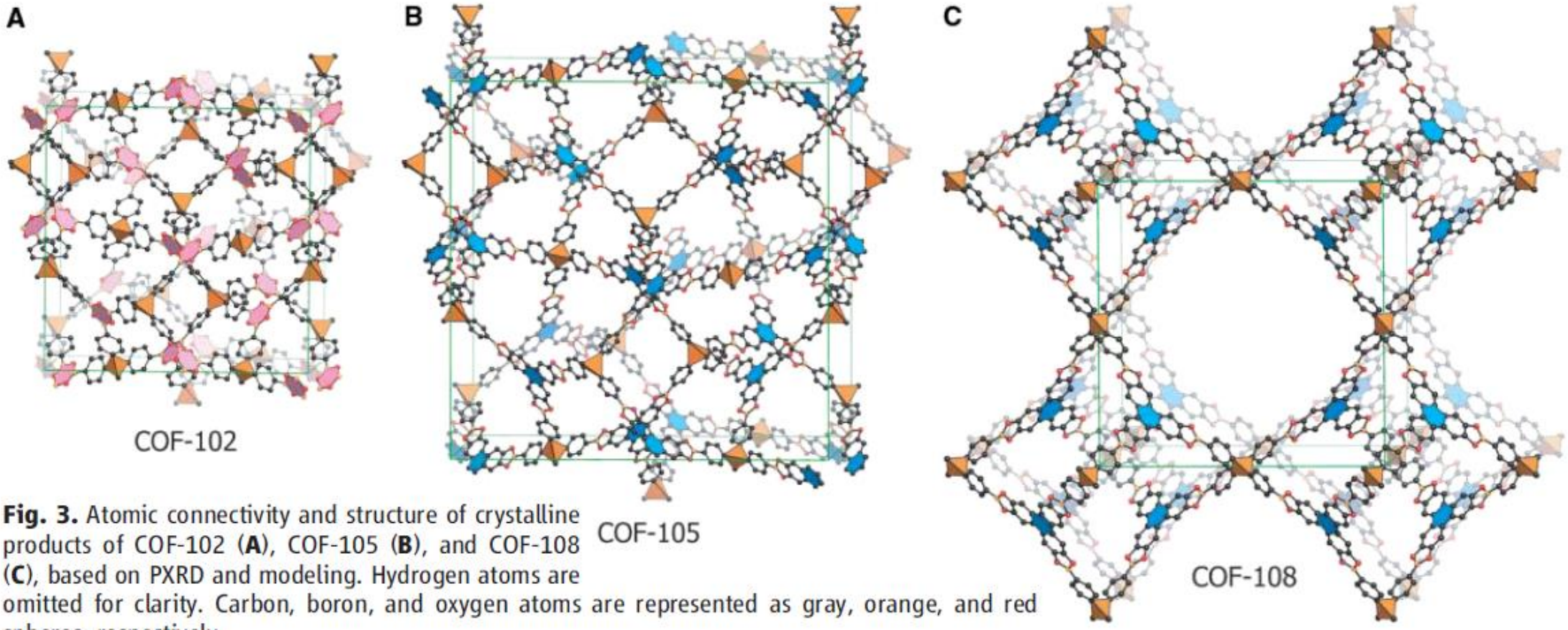

Fig. 3. Atomic connectivity and structure of crystalline products of COF-102 (**A**), COF-105 (**B**), and COF-108 (**C**), based on PXRD and modeling. Hydrogen atoms are omitted for clarity. Carbon, boron, and oxygen atoms are represented as gray, orange, and red spheres, respectively.